AD NUMBER

AD448301

NEW LIMITATION CHANGE

TO

Approved for public release, distribution unlimited

FROM

Distribution authorized to U.S. Gov't. agencies and their contractors; Administrative/Operational Use; Sep 1964. Other requests shall be referred to Army Electronics Research and Development Activity, Fort Huachuca, AZ.

AUTHORITY

USAERDA ltr, 17 Oct 1972

AD _____
USAERDAA-MET-5-64
September 1964

Numerical Solution
of the

DISTRIBUTION OF WIND AND TURBULENCE IN THE PLANETARY BOUNDARY LAYER

(Meteorological Research Notes No. 8)

By. J. F. Appleby
W. D. Ohmstede

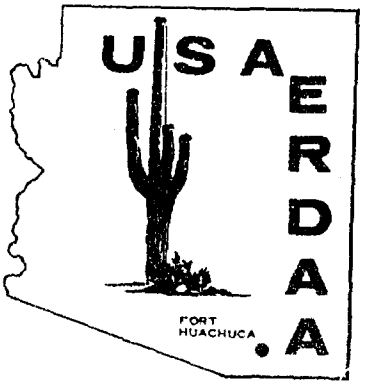

Meteorology Department

U. S. Army
Electronics Research & Development Activity, Arizona

FORT HUACHUCA

HEADQUARTERS
U. S. ARMY ELECTRONICS R&D ACTIVITY, ARIZONA
FORT HUACHUCA, ARIZONA

USAERDAA-MET-5-64, "Numerical Solution of the Distribution of Wind and Turbulence in the Planetary Boundary Layer," is published for the information of all concerned. Changes in address or attention lines should be directed to Commanding Officer, USAERDAA, ATTN: SELHU-ME, Fort Huachuca, Arizona 85613.

The findings in this report are not to be construed as an official Department of the Army position, unless so designated by other authorized documents.

"DDC AVAILABILITY NOTICE"

Qualified requesters may obtain copies of this report from the Defense Documentation Center (DDC), Cameron Station, Alexandria, Virginia. Foreign announcement and dissemination of this report is limited.

DO NOT RETURN. When no longer needed destroy in accordance with current regulations.

USAERDAA-MET-5-64
Met Rsch Notes No. 8
September 1964

NUMERICAL SOLUTION OF THE DISTRIBUTION OF WIND AND TURBULENCE IN THE PLANETARY BOUNDARY LAYER

Meteorological Research Notes No. 8

DA Task 1-A-0-11001-B-021-08

by

W. D. Ohmstede and J. F. Appleby

OBJECTIVE

The objective of DA Task 1-A-0-11001-B-021-08, "Micrometeorology", is to conduct studies dealing with the physical processes involved in the exchange of energy between the atmosphere and the earth's surface. Through such basic research, knowledge of atmospheric processes will be increased and ultimately contribute to advancing the state-of-the-art in weather forecasting.

AUTHORITY

Authority for this task is contained in letter, OCSigO, SIGRD-8b-5, dated 13 August 1957, "Proposed Coordinated Signal Corps Meteorological Program."

SUMMARY

The objective of this study is to develop a theoretical model for the structure of turbulence in the atmosphere and to solve the equations for the distribution of wind and turbulence in the planetary boundary layer. Starting with the basic equation of motion for an incompressible fluid, it is modified to incorporate the mixing-length hypothesis of Prandtl to relate the turbulent stresses to the mean flow characteristics. It is assumed the atmosphere is adiabatic, barotropic, and in a steady state. These assumptions are not all essential to the solution, but do simplify the discussion. Based on the assumptions, a relation for the mixing-length distribution within the boundary layer is developed. Using this relationship in the equation of motion led to a set of second order, nonlinear differential equations, which were solved on a digital computer. Universal profiles of the wind, stress, and eddy viscosity were fixed by invoking the important notion of similarity; that is, it is assumed the scale of turbulence is uniquely related to the gross dimensions of the boundary layer. The requisite universal constant is evaluated from experimental data. Possible applications of the model to practical problems are outlined.

TABLE OF CONTENTS

	Page
Objective and Authority	1
Summary	2
Table of Contents	3
I. Introduction	5
II. Development of the Model	6
III. Numerical Solution of Differential Equations	10
IV. Boundary Layer Model	21
V. Discussion	30
VI. Comparison with Other Models	32
VII. Conclusions	33
VIII. Bibliography	42-43
Appendix A	34
Distribution List	44-47

LIST OF ILLUSTRATIONS

Figure		Page
1	Vertical Distribution of the Mixing Length	11
2	Drag Coefficients as a Function of $G/f\ell_o$ and z/ℓ_o	18
3	Surface Wind Angle(α)as a Function of $G/f\ell_o$ and z/ℓ_o	20
4	Hf/G and $\ell_o f/G$ as Functions of Surface Rossby Number	25
5a	Surface Wind Angle (α)as a Function of the Surface Rossby Number	25
5b	Drag Coefficient (C) as a Function of the Surface Rossby Number	25
6	Hodograph of the Wind Velocity Vector	27
7	Hodograph of the Shearing Stress Vector	28
8	Vertical Distribution of the Relative Eddy Viscosity	28
9	Vertical Distribution of the Relative Viscous Dissipation	29
10	Comparison of the Drag Coefficients and Surface Wind Angles as Functions of the Surface Rossby Number for Three Models	32
11	r_o and t_o as Functions of the Surface Rossby Number	36
12	Parameters Derived from the Model vs Parameters Derived from Observations	40
13	Comparison of the Model vs Computed Eddy Viscosity (K) for Leipzig	41

Table		Page
I	Surface Rossby Number and $G/f\ell_o$ as Functions of Surface Roughness.	17
II	Vertical Distribution of Parameters Derived From the Universal Solution	23
III	Observational Data	26
IV	r, t, α, and ψ as Functions of z/ℓ_o	35
V	Leipzig Wind Profile Parameters Computed from the Model	39

NUMERICAL SOLUTION OF THE DISTRIBUTION OF WIND AND TURBULENCE IN THE PLANETARY BOUNDARY LAYER

DA Task 1-A-0-11001-B-021-08

I. INTRODUCTION

Meteorology has long been divided into the subordinate fields of macrometeorology and micrometeorology. This division has not been entirely arbitrary, for the interests and successes in these two areas have been rather widely separated. If we were to select the most characteristic elements from each of these divisions, the most logical are the geostrophic wind to characterize macrometeorology and the logarithmic wind profile for micrometeorology. Both of these relationships are rather successful formulas. The geostrophic wind equation has been used to evaluate the pressure distribution from the horizontal field of wind in the free atmosphere, whereas the logarithmic wind profile equation has been used to relate the vertical distribution of wind speed immediately above the earth's surface to the momentum transport and the roughness characteristics of the surface. On the face of it, there does not appear to be any direct connection between these two relationships for they deal with different regions of the atmosphere. However, it is the intent of this report to present a hypothesis which unifies these two concepts in such a manner as to predict the vertical distribution of wind and turbulence characteristics within a barotropic, adiabatic, steady-state planetary boundary layer.

II. DEVELOPMENT OF THE MODEL

The basic principle which is involved in this study is the equation of motion:

$$\frac{d\vec{v}}{dt} = \frac{\partial \vec{v}}{\partial t} + \vec{v} \cdot \nabla \vec{v} = -2\Omega \times \vec{v} + \vec{g} + \frac{1}{\rho} \nabla \cdot \tau \qquad (1)$$

where v is the vector wind velocity relative to a point on the earth's surface, Ω is the angular velocity of the earth's rotation, g is the acceleration of gravity, and τ is the stress dyadic. Equation (1) is notoriously difficult to solve without considerable simplification.

For this study a number of simplifying assumptions are invoked. We assume that the wind is steady and uniform in the horizontal and that quasi-hydrostatic equilibrium exists along the vertical axis. As a result, equation (1) can be written as

$$-fu = \frac{1}{\rho} \frac{\partial p}{\partial y} - \frac{1}{\rho} \frac{\partial \tau_y}{\partial z}$$

$$fv = \frac{1}{\rho} \frac{\partial p}{\partial x} - \frac{1}{\rho} \frac{\partial \tau_x}{\partial z} \qquad (2)$$

where $\vec{v} = u\vec{i} + v\vec{j}$, $f = 2\Omega \sin\theta$ where θ is the latitude, p is the pressure, and τ_x and τ_y are the stresses in the i and j directions, respectively. At this point it is possible to introduce the geostrophic wind (G) which is defined as $G = G_x \vec{i} + G_y \vec{j} = \frac{1}{\rho f}\left(\frac{\partial p}{\partial y}\vec{i} - \frac{\partial p}{\partial x}\vec{j}\right)$. Substituting in equation (2) we obtain:

$$f(G_x - u) + \frac{1}{\rho} \frac{\partial \tau_y}{\partial z} = 0$$

$$-f(G_y - v) + \frac{1}{\rho} \frac{\partial \tau_y}{\partial z} = 0 \qquad (3)$$

With few exceptions, the atmospheric boundary layer is fully turbulent and thus for practical purposes the stresses of equation (3) are wholly the Reynolds stresses. The Reynolds stresses are essentially statistical quantities that express the covariances of the turbulent fluctuations. The solution of equation (3) thus requires a knowledge of the statistical functions describing everywhere the turbulent motions. Although there have been in recent years significant advances in understanding the nature of turbulence, our knowledge still remains inadequate to derive transport relationships from the primitive equations. Consequently, almost every attempt to solve turbulent transport problems must lean heavily on semi-empirical or phenomenological theories. The "mixing-length" hypothesis of Prandtl has played the leading role in the area for three decades. This concept continues in one way or another to be used in turbulent transport models simply because it gives useful results. For this very reason, we shall utilize the mixing-length hypothesis to solve equation (3) knowing full well that the results will not be precise, but yet believing that they will be useful.

For our purposes, the mixing-length relationship can be expressed by

$$\tau/\rho = U_*^2 = \left(\ell \frac{\partial U}{\partial z}\right)^2 \qquad (4)$$

where $U_* = (\tau/\rho)^{1/2}$ is the friction velocity and ℓ is the mixing length. This expression is more commonly seen in the form:

$$\tau/\rho = U_* \ell \frac{\partial U}{\partial z} = K \frac{\partial U}{\partial z} \qquad (5)$$

where K is the eddy viscosity. There have been conflicting views as to what factors control the magnitude of the mixing length. Von Karman took the view that the magnitude of the mixing length is determined by local flow conditions. The von Karman hypothesis has certain undesirable features and in general, has not been accepted. (See Lettau[1]). On the other hand, the notion of Prandtl has generally been that the magnitude of the mixing length depends upon gross features of the flow. In the case of free turbulence, the mixing length would be assumed constant in a cross section of the mixing zone

and its magnitude proportional to the width of the mixing zone. On the other hand, in a wall turbulence regime it is assumed that the magnitude of the mixing length is proportional to the distance from the wall. For our purposes, this can be expressed by

$$\ell = kz \tag{6}$$

where k is von Kármán's constant. Using equations (4) and (6), the logarithmic wind profile for the surface boundary layer can be derived by integration, that is

$$U = \frac{U_*}{k} \ln(z/z_o) \tag{7}$$

where z_o is the roughness length.*

Neglecting the variation of density with height, we can incorporate equation (5) into equation (3) with the result:

$$\begin{aligned} f(G_x - u) + \frac{\partial}{\partial z} U_* \ell \frac{\partial v}{\partial z} &= 0 \\ -f(G_y - v) + \frac{\partial}{\partial z} U_* \ell \frac{\partial u}{\partial z} &= 0 \end{aligned} \tag{8}$$

In actuality, equation (7) is a contradiction to equation (8). The logarithmic wind profile is based on the notion that the shearing stress $U_* \ell \frac{du}{dz}$ is constant with height, whereas equations (8) clearly reveal that the vertical gradient of shearing stress is actually greatest near the boundary. This paradox can be reconciled by recognizing that the percentage rate of change of stress near the boundary is so small that for practical purposes the velocity profile is essentially logarithmic. At the other extreme of great height, the stress will vanish and by equation (8)

* A more general discussion of the roughness length can be found in ERDAA-MET-7-63 report, "A Model for Wind Flow in an Idealized Vegetative Canopy."

the wind becomes geostrophic, thus the solution of equations (8) should possess the requisite features desired in our objective.

The most notable early attempt to solve equations (8) with variable eddy viscosity was that of Rossby and Montgomery[2]. They proposed a two-layer model. In a relatively shallow layer near the ground they assumed the mixing length was linearly increasing as indicated by equation (6). The eddy viscosity was assumed to be a maximum at the top of this layer. Above this was a relatively thick transition layer in which the eddy viscosity decreases as a quadratic function of height. The model of Rossby and Montgomery was a definite improvement over previous models which assumed a constant eddy viscosity. The major criticism of the Rossby-Montgomery model is that the manner in which the eddy viscosity is specified is quite arbitrary. It is the intent of this study to obtain unified solutions of equations (8) on the basis of an assumed mixing-length distribution. It is proposed that on the basis of similarity the magnitude of the mixing length is determined by gross features of the flow.

III. NUMERICAL SOLUTION OF DIFFERENTIAL EQUATIONS

According to equation (5) the eddy viscosity is equal to the product of the friction velocity and the mixing length, and according to equation (4) the friction velocity depends on the mixing length and the wind shear. In the surface boundary layer the friction velocity behaves as if it were nearly independent of the height, whereas at great height the wind approaches the geostrophic wind and the friction velocity becomes negligible. On the other hand, the mixing length, according to equation (6) should be valid ad infinitum. The outer portion of the boundary layer behaves more like a region of free turbulence than of wall turbulence, and consequently, one would be led to propose that the mixing length approaches a limiting value in the layers remote from the boundary.

In this study, it is proposed that when the planetary boundary layer is in an adiabatic steady state, the mixing length increases with height at the rate given by von Karman's constant, but that there is a direct linear feedback which prevents unbounded growth. This notion is expressed by the following differential equation:

$$\frac{d\ell}{dz} = k - \ell/L \tag{9}$$

where L is a constant.
The solution of equation (9) statisfying the boundary conditions is:

$$\ell = \ell_o(1-e^{-z/L}) \tag{10}$$

where $\ell_o/L = k$. This equation has the characteristics that ℓ essentially increases linearly with height near the boundary, but approaches the limiting value ℓ_o at great height. Figure 1 compares equation (1) with the mixing-length distribution as computed from Lettau's[3] reanalysis of the Leipzig wind profile. Equation (10) fits the data reasonably well except in the upper portion of the profile. However, in this region the evaluation of the mixing length is much less reliable because of the small values of the velocity derivative.

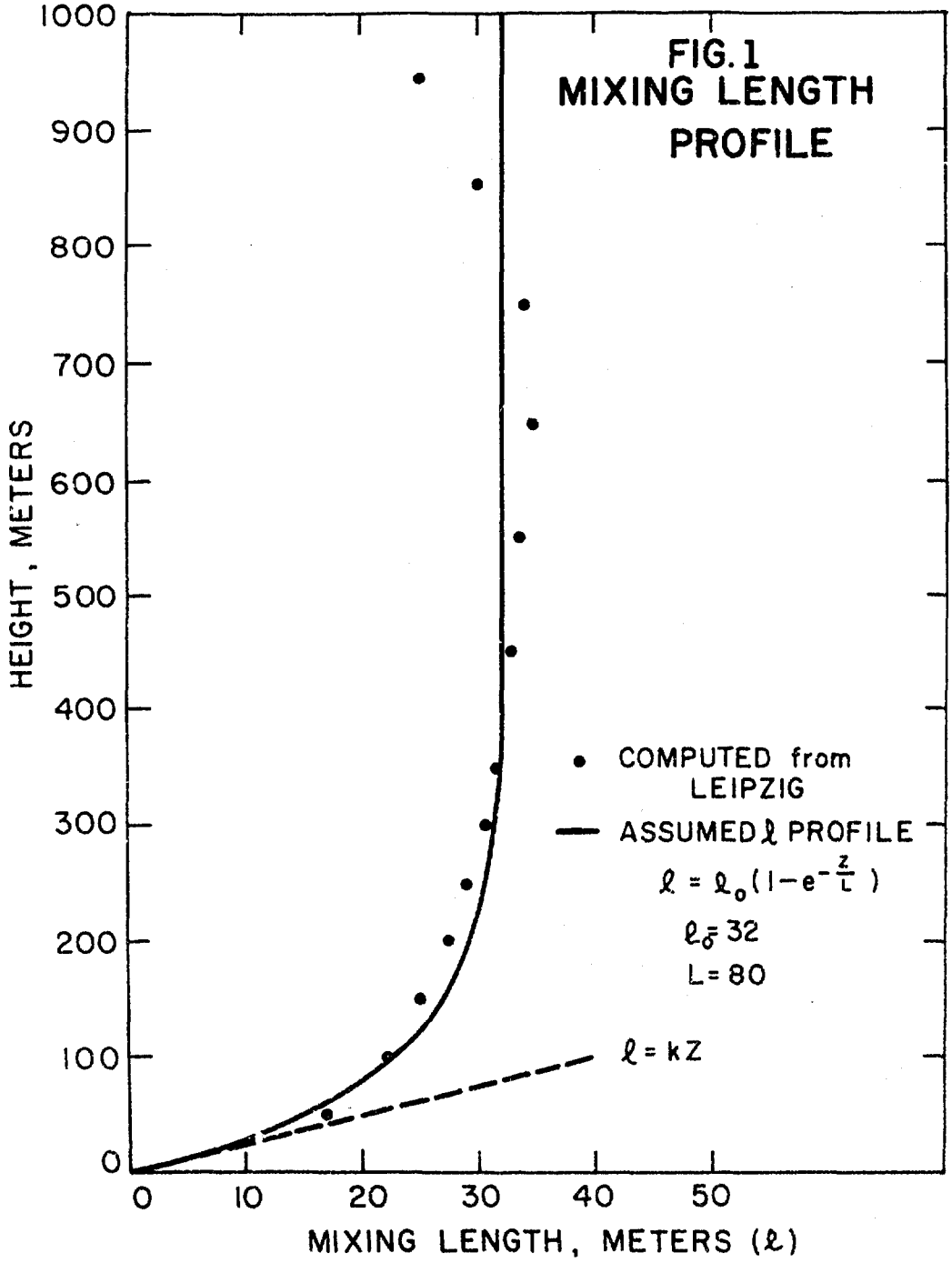
FIG. 1
MIXING LENGTH
PROFILE
HEIGHT, METERS
1000
900
800
700
600
500
400
300
200
100
0
0
10
20
30
40
50
MIXING LENGTH, METERS (ℓ)
COMPUTED from LEIPZIG
ASSUMED ℓ PROFILE
$\ell = \ell_0(1-e^{-\frac{z}{L}})$
$\ell_0 = 32$
L = 80
$\ell = kZ$

For this study equation (10) has been utilized as a general expression for the mixing length. Having this expression it is possible to solve for the velocity profile in the planetary boundary layer. For computational purposes, it is necessary to express the equation in nondimensional form. For this purpose we define the following variables:

$$U = (G_x - u)/G, \quad V = (G_y - v)/G, \quad s = \tau_x/\rho G^2, \quad t = \tau_y/\rho G^2,$$

$$T = U_*/G = (s^2 + t^2)^{1/4} \qquad R_o = G/fz_o \qquad x = z/z_o$$

where R_o is termed the Rossby number. Using these expressions, equations (3) can be expressed as

$$V = R_o \frac{\partial s}{\partial x}, \quad U = - R_o \frac{\partial t}{\partial x} \tag{11}$$

and equation (5) can be expressed as

$$s = - T(\ell_o/z_o)\gamma \frac{\partial U}{\partial x}, \quad t = - T(\ell_o/z_o)\gamma \frac{\partial V}{\partial x} \tag{12}$$

where $\gamma = 1 - \exp(-z/L)$. If we differentiate equations (11) and substitute the results in equations (12), we obtain

$$s = A_o T\gamma \frac{\partial^2 t}{\partial x^2}, \quad t = - A_o T\gamma \frac{\partial^2 s}{\partial x^2} \tag{13}$$

where $A_o = R_o \ \ell_o/z_o$. Equations (13) are the basic equations to be solved for the boundary layer model. The boundary condition requires that $s = t = o$ at great height and we chose axes of orientation such that at the lower boundary $t = o$ and $s = s_o$. For each value of the parameter A_o, there must be a corresponding value of s_o. However, the actual relationship of s_o to A_o cannot be determined until the solutions are known. To obviate this paradox it is necessary to rewrite equations (13) in a form containing only a single parameter. This was done by defining new variables as follows:

$$P = \frac{A_o T}{10^{12}}, \quad Q = \left(\frac{A_o}{10^{12}}\right)^2 s, \quad R = \left(\frac{A_o}{10^{12}}\right)^2 t$$

Utilizing these terms, equations (13) become

$$Q = 10^{12} P_\gamma \frac{\partial^2 R}{\partial x^2} \; ; \quad R = - 10^{12} P_\gamma \frac{\partial^2 Q}{\partial x^2} \tag{14}$$

with the following boundary conditions

$$x = 1 \qquad Q = Q_o \qquad R = 0$$

$$x \to \infty \qquad Q = R = P = 0$$

From equation (14) and the boundary conditions, it can be seen that a particular solution is completely specified by the quantity Q_o provided γ is solely a function of proximity to the boundary.

Considerable difficulty was encountered in solving equations (14). It was necessary to assume that Q and R became negligible at a finite but large height H rather than at infinity. Numerous mathematical methods were tried to solve the equations, but the solutions were finally achieved more by utilizing physical intuition than mathematical prowess. Briefly, the method of solution consisted of transforming the independent variable to $y = 2.0\ x$ and then establishing a grid of 100 equally spaced points in the y domain between $x = 1$ and $x = H$. The derivatives at the grid points were approximated from second-order Lagrangian polynomials utilizing the values of the variables at adjacent grid points. On the basis of the ordinary differential equations, a form of parabolic partial differential equation was assumed and the final solution was derived through integration until the solution of the partial differential equations decayed to the steady state ordinary solution.

Choosing $z_o/\ell_o = 3.125 \times 10^{-5}$, numerous solutions of equations (14) were computed for boundary conditions of Q_o ranging over three orders of magnitude. The solutions can be applied to any arbitrary roughness by accepting as the boundary condition the values of Q and R at the corresponding height in the solutions. The roughness plays a significant role in translating the solutions of Q and R into terms of real physical variables. By definition, we know that the real velocity is zero at the roughness height z_o. In terms of the

nondimensional variables this means that $u^2 + v^2 = 1$. This can be expressed according to equation (10) as $R_o^2 \left(\frac{\partial s}{\partial x}\right)^2 + \left(\frac{\partial t}{\partial x}\right)^2 = 1$. This equation can be used to determine the surface Rossby number, R_o, for a given solution at any roughness z_o by the equation

$$R_o (\ell_o/z_o)^2 = \left(\frac{\partial Q^2}{\partial x} + \frac{\partial R^2}{\partial x}\right)^{1/2} \tag{15}$$

or the quantity $G/f\ell_o = (z_o/\ell_o)^3 \left(\frac{\partial Q^2}{\partial x} + \frac{\partial R^2}{\partial x}\right)^{1/2}$ (16)

From a practical standpoint it was found that the evaluation of the derivatives of Q and R at the lower boundary could not be adequately determined from finite difference formulas. Consequently, an approximate analytical solution was developed. Q and P are nearly invariant with height near the lower boundary. Therefore, we can express Q and P in terms of their average value between adjacent grid points in the first meter above the lower boundary. Furthermore, we know from equation (6) that $\gamma = (z_o/L)x$ near the boundary. Consequently, the first equation of equations (14) can be approximately expressed as

$$\frac{\partial^2 R}{\partial x^2} = \frac{L\bar{Q}}{10^{12}\bar{P}z_o} \frac{1}{x} \tag{17}$$

where the bar designates average values. If we integrate equation (17), we obtain (let $\frac{L\bar{Q}}{10^{12}\bar{P}z_o} = A$)

$$\frac{\partial R}{\partial x} = \frac{\partial R_1}{\partial x} + A \ln x \tag{18}$$

where the subscript 1 refers to the lower boundary at which $x = 1$. Integrating equation (18) we obtain

$$R = R_1 + \frac{dR_1}{dx}(x - 1) + A(x \ln x - x + 1) \tag{19}$$

If R and x correspond to the first grid point above the boundary, then the derivative at the boundary can be evaluated by

$$\frac{dR_1}{dx} = \frac{R_2 - R_1}{x_2 - 1} - A\left[\frac{x_2 \ln x_2}{(x_2 - 1)} - 1\right] \qquad (20)$$

where $\bar{P}$ and $\bar{Q}$ are the average values of Q and P in the layer from x = 1 to x_2.

Using equation (19) we can express the second of equations (14) as (let $\frac{L}{10^{12}\bar{P}z_c} = B$)

$$\frac{\partial^2 Q}{\partial x^2} = -B\left[\frac{R_1}{x} + \frac{\partial R_1}{\partial x}\left(1 - \frac{1}{x}\right) + A\left\{\ln x + \left(\frac{1}{x} - 1\right)\right\}\right] \qquad (21)$$

Integrating equation (21) we obtain

$$\frac{\partial Q}{\partial x} = \frac{\partial Q_1}{\partial x} - B\left[\left(R_1 + A - \frac{\partial R_1}{\partial x}\right)\ln x + A\{x \ln x - (x - 1)\} + \left(\frac{\partial R_1}{\partial x} - A\right)(x - 1)\right] \qquad (22)$$

Integrating equation (22) we obtain

$$Q = Q_c + \frac{\partial Q_1}{\partial x}(x - 1) - B\left[\left(R_1 + A - \frac{\partial R_1}{\partial x}\right)\{x \ln x - (x - 1)\} + \frac{A}{2}\left\{x^2 \ln x - \frac{(x - 1)(x + 1)}{2} - (x - 1)^2\right\} + \left(\frac{\partial R_1}{\partial x} - A\right)\frac{(x - 1)^2}{2}\right] \qquad (23)$$

Using the values of $\hat{q}$ and x at the second grid point, the first derivative can be evaluated by

$$\frac{d\hat{q}_1}{dx} = \frac{\hat{q}_2 - \hat{q}_1}{x_2 - 1} + B\left[\left(R_1 - \frac{\partial R_1}{\partial x} + A\right)\left(\frac{x_2 \ln x_2}{x_2 - 1} - 1\right)\right.$$

$$\left. + \frac{A}{2}\left(\frac{x^2_2 \ln x_2}{x_2 - 1} - \frac{3x_2}{2} + \frac{1}{2}\right) + \left(\frac{\partial R_1}{\partial x} - A\right)\frac{x_2 - 1}{2}\right] \tag{24}$$

The second term on the right of equation (24) is generally nearly trivial in comparison with the first term. The numerical values of the derivatives obtained from equations (20) and (24) can be used to evaluate the derivatives at any arbitrary height x from equations (18) and (22). Therefore, the Rossby number and G/f can be determined for any arbitrary roughness length from equations (15) and (16). Table I presents the values of the Rossby number and $G/f\ell_o$ for various roughness lengths as determined from the various solutions. It is to be noted that for each solution $G/f\ell_o$ decreases with increasing roughness.

A graphical representation of u_*/G as a function of $G/f\ell_o$ and z_o/ℓ_o is presented in Figure 2. The quantity $u_*/G \equiv C$ is analogous to a drag coefficient. From Figure 2 the magnitude of u_*/G can be determined for any combination of $G/f\ell_o$ and z_o/ℓ_o. Thus, the surface shearing stress can be determined when the geostrophic wind is known; that is,

$$\tau_o = \rho C^2 G^2 \tag{25}$$

The angle between the surface wind and the geostrophic wind can be evaluated by

$$\alpha = \arctan \frac{\partial \hat{q}}{\partial x} \Big/ \frac{\partial R}{\partial x} - \arctan (R/_Q) \tag{26}$$

where the derivatives are referred to the roughness height.

TABLE I
Values of the Surface Rossby Number and $G/f\ell_o$ for Various Roughness Lengths from Three Solutions

	$Q_o = 3.2\times10^{-2}$		$Q_o = 2.65\times10^{-2}$		$Q_o = 1.0\times10^{-2}$	
z_o/ℓ_o	$R_o\times10^8$	$G/f\ell_o\times10^3$	$R_o\times10^8$	$G/f\ell_o\times10^3$	$R_o\times10^8$	$G/f\ell_o\times10^3$
3.125×10^{-6}	25.4722	7.960	22.8870	7.152	13.2245	4.133
9.375×10^{-6}	7.9973	7.497	7.1791	6.730	4.1295	3.871
3.125×10^{-5}	2.2378	6.993	2.0066	6.270	1.1147	3.586
9.375×10^{-5}	.6972	6.535	.6243	5.853	.3549	3.328
3.125×10^{-4}	.1932	6.039	.1728	5.400	.0975	3.046
9.375×10^{-4}	.0596	5.590	.0532	4.990	.0298	2.791
3.125×10^{-3}	.0163	5.104	.0145	4.547	.0080	2.515
9.375×10^{-3}	.0047	4.435	.0042	3.935	.0028	2.139
3.125×10^{-2}	.0013	3.951	.0011	3.493	.0006	1.862

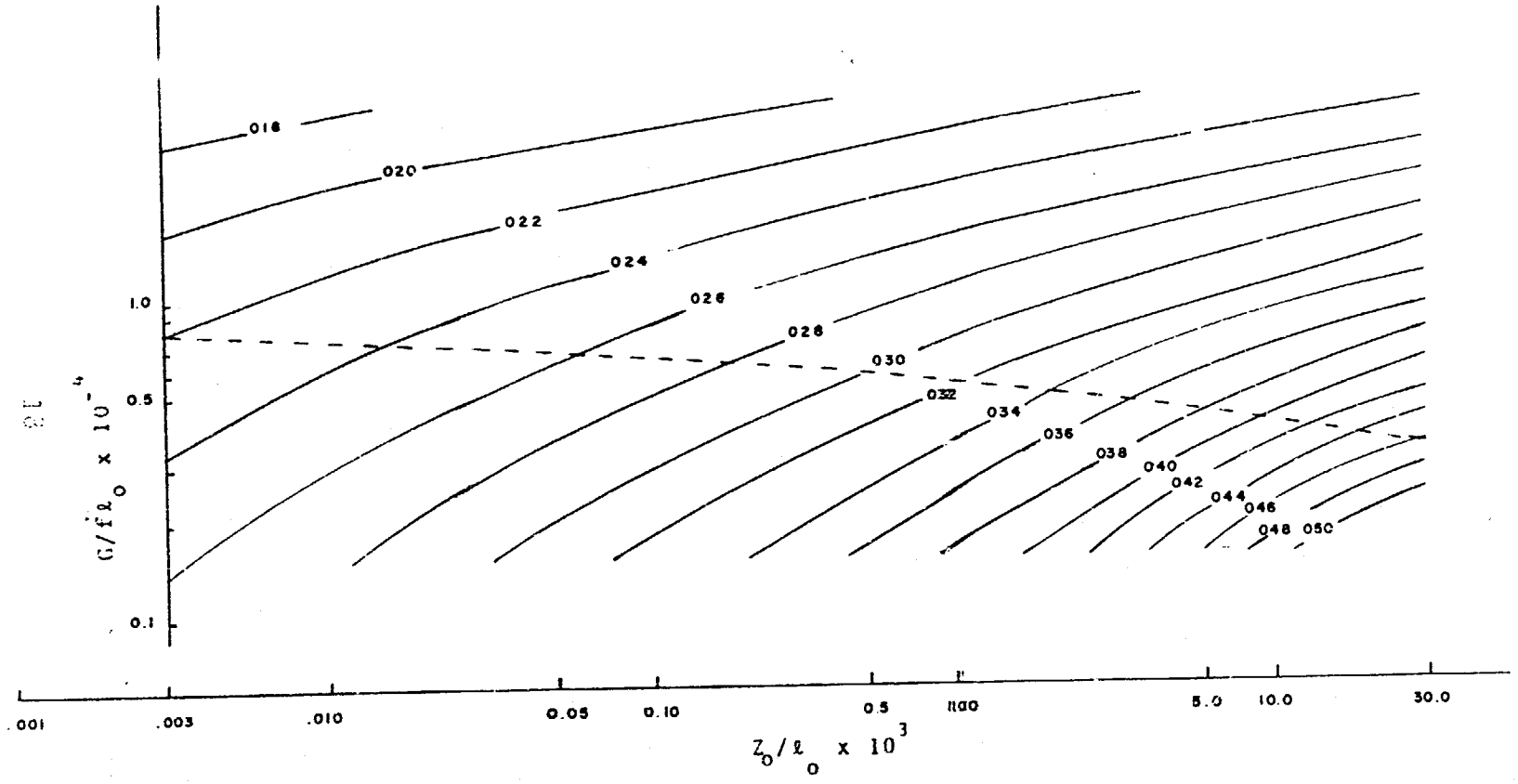

FIG. 2 Drag Coefficient U_*/G as a Function of $G/f\ell_o$ and z_o/ℓ_o

_____ RELEVENT SOLUTION

Figure 3 represents a graphical representation of α as a function of $G/f\ell_o$ and z_o/ℓ_o.

According to equations (11) the velocity defects (U, V) are proportional to the derivatives of the shearing stress components. These derivatives were determined from the approximate analytical solution near the surface and the remaining derivatives at grid points were approximated from second-order Lagrangian polynomials using values at adjacent grid points. Once the derivatives are determined and the surface Rossby number is computed from equation (15) the vertical distribution of the velocity defects can be computed. From the determined variables the normalized stresses, friction velocity, and eddy viscosity distributions can also be found. These parameters were tabulated for each of the solutions.

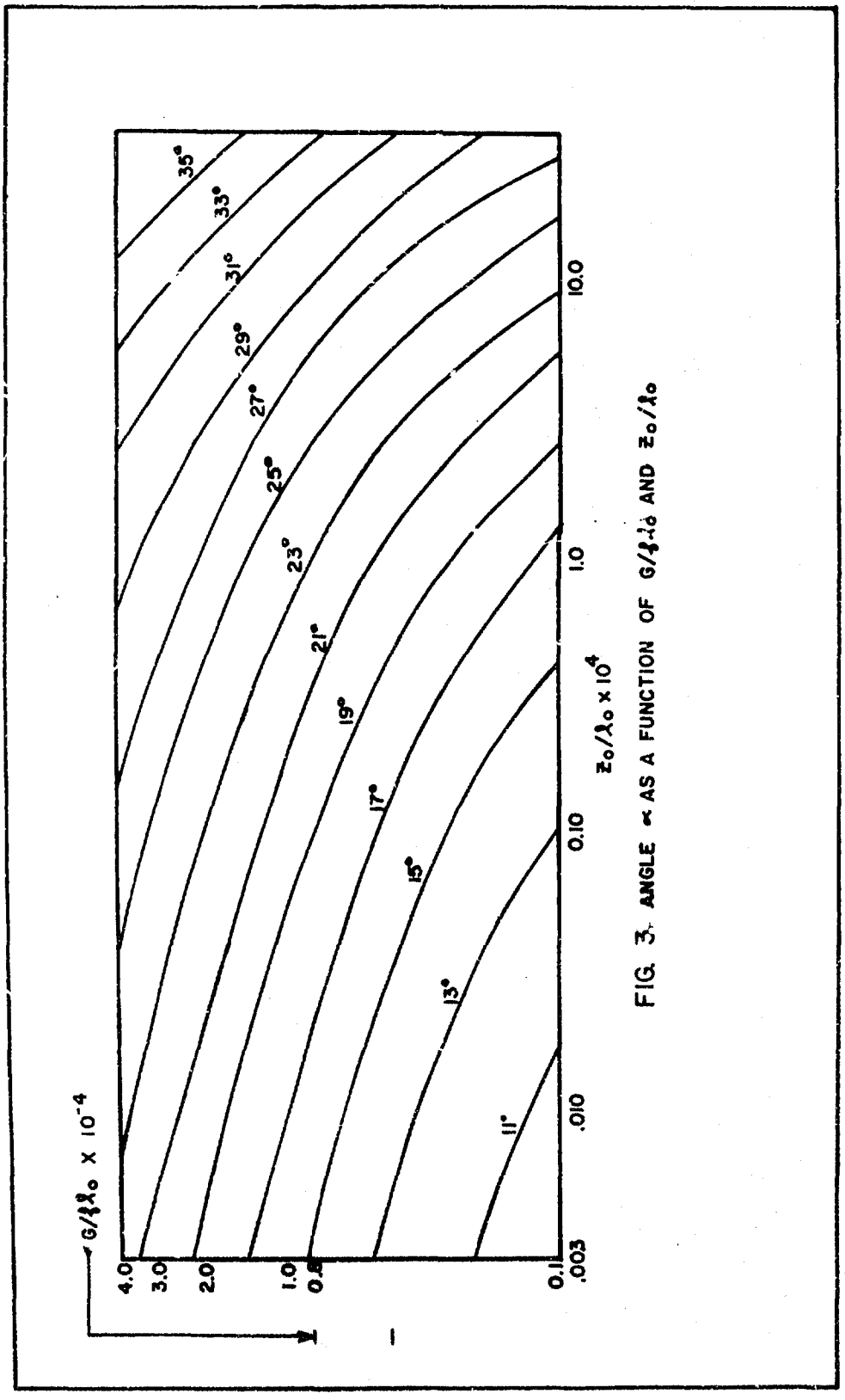

FIG. 3. ANGLE α AS A FUNCTION OF $G/4\lambda_0$ AND Z_0/λ_0

IV. BOUNDARY LAYER MODEL

To this point we have been purely formal in that we have stated the requisite differential equations, postulated a particular functional form for the mixing length, and then proceeded to find a number of solutions of the equations using the assumed mixing-length relationship. The next important question is Which of these solutions are relevant to the real atmospheric planetary boundary layer? In attempting to answer this question we shall invoke the important notion of similarity. Briefly, we assume that the Reynolds number of the planetary boundary layer is so large that there exists a universal equilibrium structure for the turbulent eddies, and that the scale of the turbulent eddies as measured by the mixing length is universally related to the gross scale (depth) of the boundary layer for any given Rossby number. It remains to determine what scale parameters are to be used to measure the eddy sizes and boundary layer depth. It is immediately apparent from equation (10) that either ℓ_o or L is adequate to characterize the eddy structure; however, the selection of a characteristic scale length for the boundary layer is somewhat more difficult. The following lists some of the possible scale heights:

$$H_1 = G/f$$

$$H_2 = u_*/f$$

$$H_3 = h \text{ (gradient wind level)}$$

$$H_4 = (G/f)\, C^2$$

$$H_5 = (G/f)\, C^2 \cos\alpha$$

$$H_6 = (G/f)\, C^2 \sin\alpha$$

A relationship such as H_1 was used in the first paper by Blackadar[4], but his second report[5] used a relation that can be reduced to H_2. H_3 is a simple and direct scale length analogous to the boundary layer depth in fluid mechanics. H_4 is the ratio of surface stress to pressure gradients, i.e., $\tau_o/(\partial p/\partial y)$. H_5 is an integral scale which can be shown to be equivalent to $H_5 = \int_o^\infty (v/G)dz$, that is, the integral of the normalized

cross-isobaric flow. This scale height has the interesting property that ρGH_5 is the total mass transfer across the isobars. H_6, another integral scale, is equivalent to $\int_0^\infty (u/G)dz$, the integral of the isobaric flow and ρGH_6 is the total mass transport along the isobars. There is no *a priori* reason for selecting one scaling length over another. Hence a comparison of two basic parameters that result from the model was made for each of the scaling lengths. These are the relationships between the angle (α) and the geostrophic drag coefficient, respectively, and the surface Rossby number.

H_1 tends to result in higher than observed drag coefficients at high surface Rossby numbers, although α's are quite small as observed. H_2 and H_3 give nearly the same results and give more reasonable drag coefficients, but slightly larger angles. H_4 and H_5 again give comparable results. The drag coefficients are more in agreement with observations, but the α's again are larger than observed. H_6 gives a drag coefficient in closer agreement with observations, but has the poorest agreement for α's.

We have selected H_3 as our characteristic length scale because of its simplicity and because preliminary results show its adaptability to the thermal wind case.

According to our notion of similarity, the quantity (H_3/ℓ_o), representing the ratio of the length scale of the boundary layer and the length scale of the eddy structure, is a universal constant. To determine its magnitude we resort to the data from the Leipzig wind profile. These data are H_3 = 1070m and ℓ_o = 32m with the result that H_3/ℓ_o = 33.44. With this constant we are able to select the solution which is proposed as the universal solution of the steady state, barotropic, neutral planetary boundary layer. Table II presents this solution in terms of the nondimensional variables.

We can now demonstrate how this solution is used to determine the distribution of wind and turbulence in the planetary boundary layer. We can also illustrate some salient features of the model. To use the model, it is necessary to specify the three parameters which determine the surface Rossby number—namely, the geostrophic wind, the latitude, and the surface roughness.

Table II

Basic Model Solution as a Function of Relative Height

z/ℓ_o	$(U_G-u)/G$	$(V_G-v)/G$	$\tau_x/\rho G^2 \times 10^3$	$\tau_y/\rho G^2 10^3$	U_*/G	$K/\ell_o G$
53.1	.0000	.0000	.0000	.0000	.0000	.0000
50.0	.0021	-.0009	.0007	.0005	.0009	.0010
45.0	.0043	.0052	.0005	.0035	.0019	.0019
40.0	-.0030	.0147	-.0080	.0048	.0031	.0031
35.0	-.0112	.0174	-.0151	.0020	.0039	.0047
30.0	-.0465	+.0030	-.0316	-.0319	.0067	.0067
25.0	-.0653	-.0306	-.0218	-.0772	.0089	.0090
20.0	-.0676	-.0809	.0213	-.1315	.0115	.0115
15.0	-.0429	-.1411	.1096	-.1781	.0144	.0144
10.0	.0099	-.2011	.2472	-.1942	.0177	.0174
6.4	.0711	-.2381	.3741	-.1719	.0203	.0187
5.0	.1010	-.2503	.4285	-.1527	.0213	.0184
2.5	.1724	-.2690	.5327	-.0988	.0233	.0147
1.0	.2460	-.2787	.5978	-.0503	.0245	.0081
.5	.2956	-.2819	.6200	-.0283	.0249	.0045
0.25	.3420	-.2835	.6317	-.0162	.0251	.0024
0.10	.3999	-.2845	.6383	-.0028	.0252	.0010
1.0×10^{-2}	.5670	-.2853	.6419	.0000	.02534	.00009
1.0×10^{-3}	.7370	-.2855	.6426	.0000	.02535	.00002
1.0×10^{-4}	.8830	-.2855	.6427	.0000	.02535	.000004
1.0×10^{-5}	1.229	-.2855	.6428	.0000	.02535	.000000
1.0×10^{-6}	1.173	-.2855	.6428	.0000	.02536	.000000

The geostrophic wind can be readily evaluated from synoptic (or prognostic) weather maps, while several sources [6-7] can be consulted to evaluate the roughness at the site.

The relationship of Hf/G and $\ell_o f/G$ to the surface Rossby number as derived from the model is illustrated in Figure 4. The magnitude of ℓ_o and H can be determined from Figure 4; consequently, the nondimensional height (z/ℓ_o) of Table II can be converted to true height z. Details of the computation of this and other dimensional parameters for the boundary layer are given in Appendix A. From Figure 4 it can be seen that for a fixed (G/f), an increase in roughness increases the depth of the boundary layer (H) and the limiting mixing length (ℓ_o). In a like manner, for a fixed roughness, an increase in the geostrophic wind increases (H) and (ℓ_o). Decreasing the latitude tends to increase these parameters. It should be noted that the boundary layer depth is rather insensitive to roughness.

We can also determine the relationship of the angle of the surface wind and the geostrophic drag coefficient to the surface Rossby number. The model relationships are illustrated by the curves of Figure 5. In addition, all known observations (Table III) have been plotted to permit comparison with the results of the model. Small angles of the surface wind are associated with strong geostrophic winds, low latitude, and small roughness. The trend of the geostrophic drag coefficient is similar to that of the surface wind. Unlike fully turbulent flow in ducts, the drag coefficient of the planetary boundary layer is not independent of the flow velocity; thus, the surface shearing stress as evaluated from equation (19) is not proportional to the square of the geostrophic wind, but to a power less than two. Comparing Figure 4 with Figure 5, it is apparent that the surface wind angle and the geostrophic drag coefficient are less sensitive to changes in G/f than are H and ℓ_o. With the exception of the Leipzig wind profile, the available data do not satisfy the conditions of the model (barotropic, neutral, steady state) or the method of computation used to analyze the data is of doubtful validity. There is qualitative agreement between the model and the observations, but the scatter is too great and the observations are too few to permit a formal statistical analysis of the results.

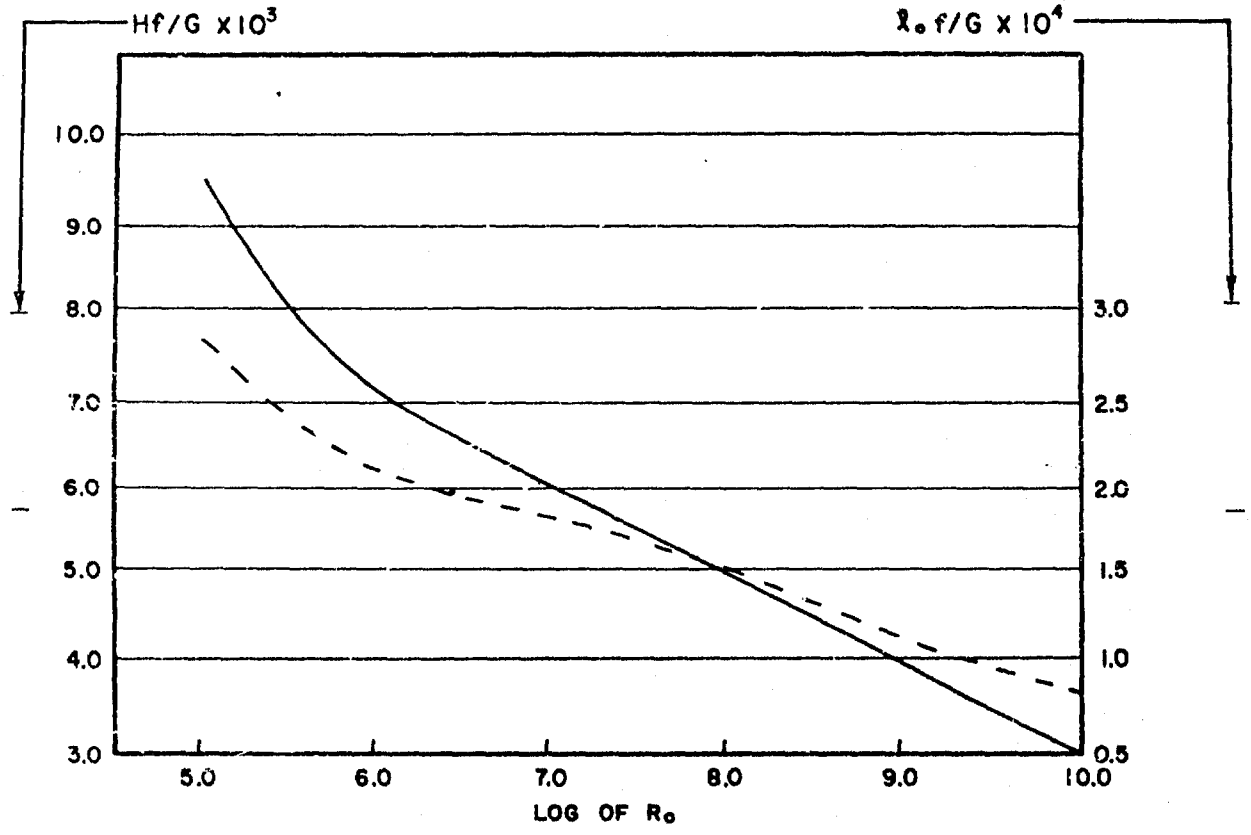

FIG. 4 Hf/G AND $\ell_0 f/G$ AS FUNCTIONS OF THE SURFACE ROSSBY NO.

——— Hf/G ---- $\ell_0 f/G$

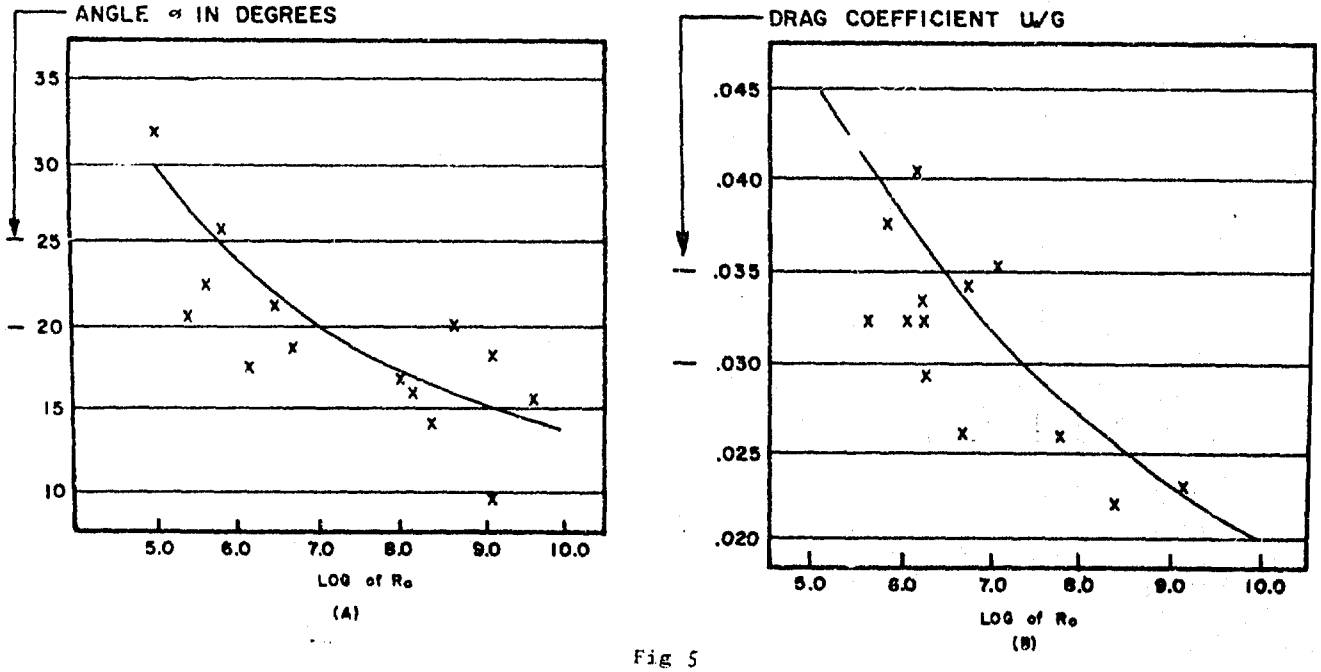

Fig 5

MODEL RELATIONSHIPS vs OBSERVATIONS

_____ MODEL x OBSERVATIONS

TABLE III

OBSERVATIONAL DATA

	G/f(m)	Z_o(cm)	Observed α	Observed Drag Coefficient
(1) Leipzig	7.75×10^5	.20	26.1	.03722
(1) Scilly I	1.098×10^5	.05	13.9	.022
(1) Scilly II	5.90×10^4	.05	9.5	.023
(2) Dobson I	4.04×10^4	3.2	13.0	-----
(2) Dobson II	8.0×10^4	3.2	21.5	-----
(2) Dobson III	1.37×10^5	3.2	20.0	-----
(3) Ellendale	1.01×10^5	2.3	18.6	.034
(3) Drexel	1.18×10^5	9.5	18.7	.032
(3) Broken Arrow	1.34×10^5	38.5	22.4	.032
(3) Groesbeck	1.46×10^5	67.5	20.9	.034
(2) Jeffries I	3.36×10^4	.001*	15.7	-----
(2) Jeffries II	8.66×10^4	.008*	18.2	-----
(2) Jeffries III	1.28×10^5	0.13*	17.2	-----
(2) Jeffries IV	1.68×10^5	0.15*	16.2	-----
(1) Quickborn	8.53×10^4	5.0	----	.0358
(1) Cambridge	7.81×10^4	.15	----	.0257
(1) O'Neil	1.49×10^5	0.9	----	.033
(1) College Station I	1.37×10^5	.3	----	.026
(1) College Station II	1.37×10^5	.6	----	.029
(1) College Station III	2.055×10^5	1.8	----	.032
(1) College Station IV	3.28×10^5	3.3	----	.035
(1) Munich Forrest I	4.65×10^4	20.0	----	.048
(1) Munich Forrest II	1.39×10^5	10.0	----	.040
(4) Brookhaven	1.05×10^5	100.0	32	.035

Source:
1. Lettau
2. Rossby, Montgomery
3. Johnson, Warren B.
4. Blackadar

* Established from Deacon's relationships for wind speed vs sea surface roughness.

Graphic presentations of salient features of the model are presented in Figures 6 through 9. Figure 6 is a hodograph of the wind vector in arbitrary units. To use the graph a line is drawn, as illustrated in the figure, from the origin to the point on the hodograph corresponding to the value of z/ℓ_o. This line represents the geostrophic wind vector. The velocity at any arbitrary height z is determined by drawing a line from the point on the hodograph corresponding to z_o/ℓ_o to the desired z/ℓ. In a similar manner, the hodograph of the shearing stress vector is shown in Figure 7. To determine the magnitude of the surface stress, we obtain the geostrophic drag coefficient from Figure 5b and then use equation (19).

Figure 8 shows the vertical distribution of the relative eddy viscosity $k/\ell_o G$. From previous discussion we concluded that for a fixed roughness and latitude, ℓ_o increases with increasing geostrophic wind. Therefore, the eddy viscosity is proportional to the geostrophic wind to a power greater than one. A simple computation shows that the maximum of eddy viscosity occurs at a height approximately one-fifth of the gradient level. Figure 9 is a graphic representation of the vertical distribution of the relative viscous dissipation ($\varepsilon \ell_o / G^3$).

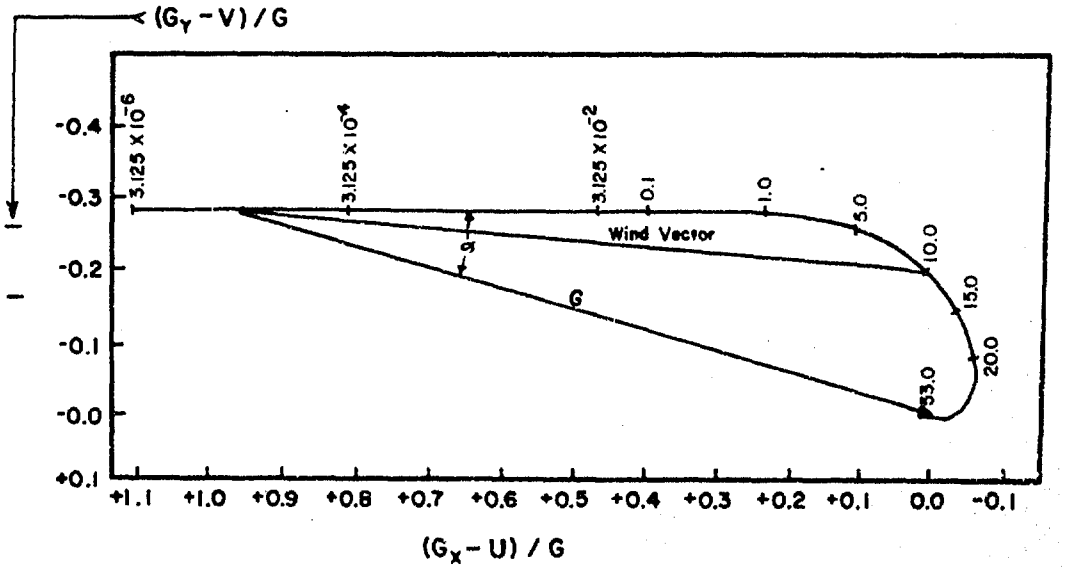

FIG. 6 WIND VELOCITY HODOGRAPH

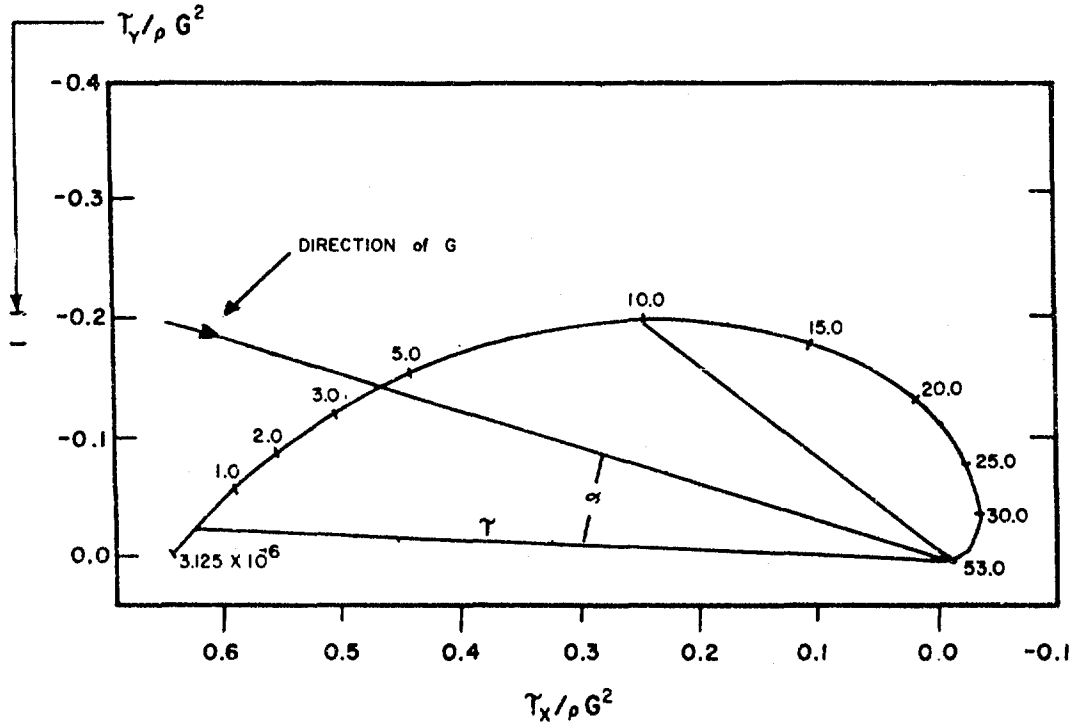

FIG. 7 SHEARING STRESS HODOGRAPH

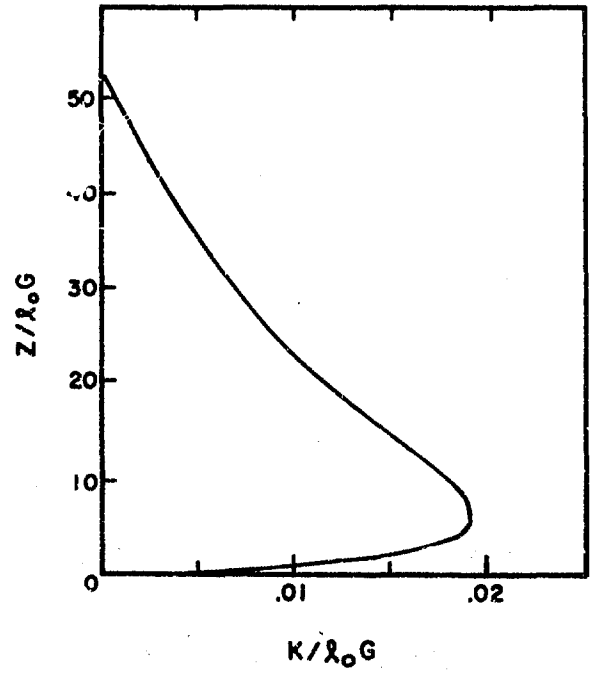

FIG. 8 RELATIVE EDDY VISCOSITY

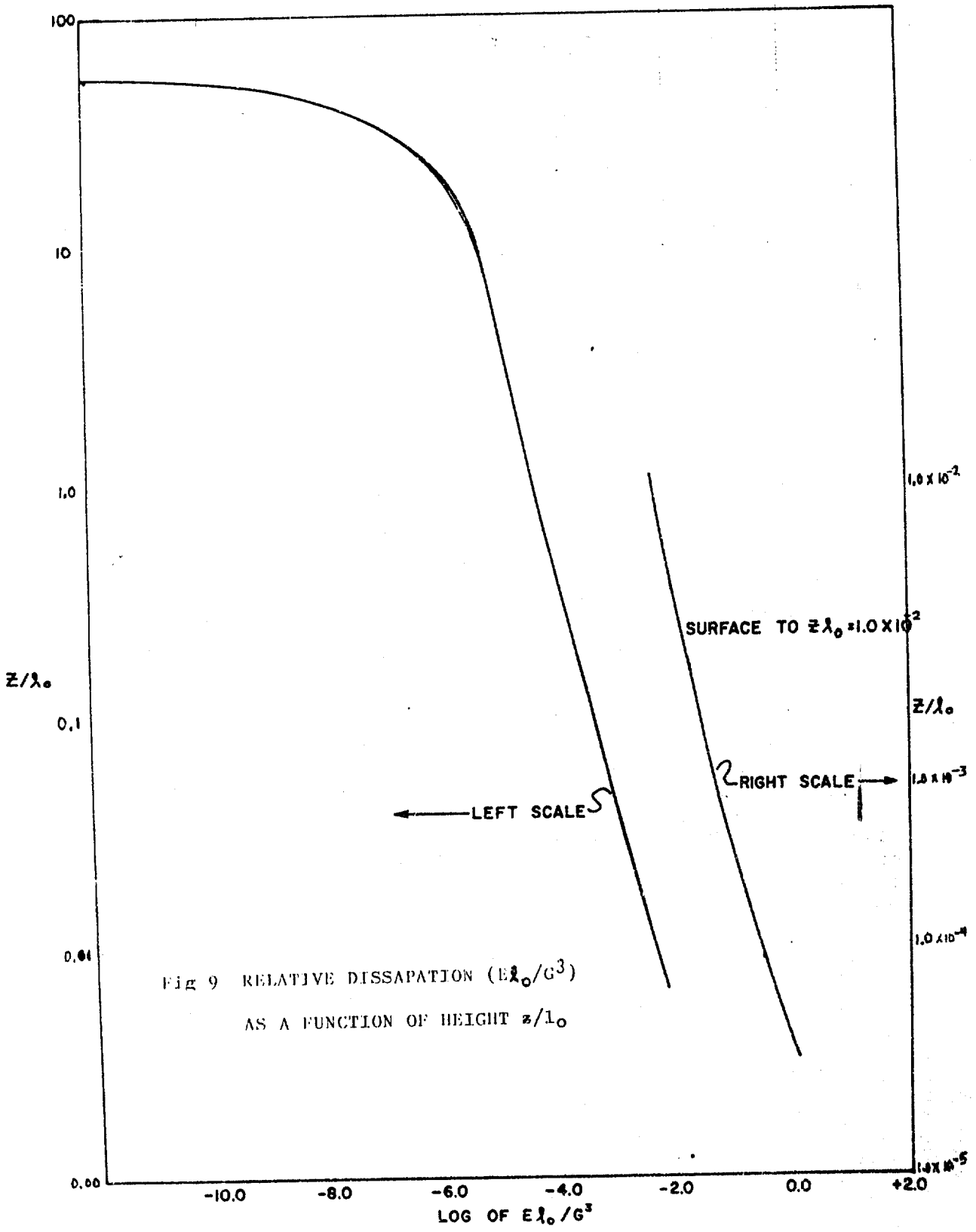

Fig 9 RELATIVE DISSAPATION ($E\lambda_o/G^3$)
AS A FUNCTION OF HEIGHT z/l_o

V. DISCUSSION

The planetary boundary layer model which has been presented contains the features sought in the objective. In the free atmosphere, the wind approaches the geostrophic wind, while in the surface boundary layer the vertical distribution of wind is logarithmic. However, it would be misleading to imply from this that the idealized planetary boundary layer model could be as successful as these two otherwise independent concepts. The success of the geostrophic wind equation lies in the fact that the wind appears to respond quickly to pressure gradient changes, with the result that the wind is quasi-geostrophic in the free atmosphere even when conditions are not ideal. In like manner, the wind profile responds quickly to stress and roughness changes in the surface boundary layer. However, Batchelor (Reference [8], p. 256) has emphasized that the stress at the ground is likely to respond to pressure gradient changes slowly, with the result that a true steady-state planetary boundary layer would be a rare phenomenon in the real atmosphere. In reply, Lettau (Reference [8], p. 257) has stated that in the lower portion of the boundary layer the profile will respond relatively quickly to pressure gradient changes, but more prolonged inertial oscillations will complicate the upper portion of the boundary layer.

In the course of solving equations (13), the authors met a problem of computational instability in the upper portion of the boundary layer solution. This instability had all the appearances of inertial oscillations of the type expected by Lettau. However, in spite of these oscillations, the lower portion of the profile was stable and the distribution of stress was in consonance with the steady-state solution. This result is rather encouraging; it implies that at the boundary such features as the stress and angle of the wind are in balance with the geostrophic wind, even if the upper portion of the boundary layer remains in oscillation. In any event, the assumption of steady-state sets a restriction on the utility of the boundary layer solutions. A quantitative evaluation of this limitation would require that the "time constant" of the boundary layer be evaluated through non-steady solutions.

The restriction of the model to adiabatic conditions is another obvious limitation of the model. A steady-state neutral boundary layer model is not likely to be applicable to clear sky conditions over land. However, it should be often applicable to conditions over the sea or over land surfaces with overcast skies.

The restriction of the solutions to barotropic conditions was not essential, but it did greatly simplify the problem in terms of the number of solutions required. Furthermore, it would seem that for the case of constant thermal wind, the boundary layer model in terms of the deviation of the wind from the geostrophic wind would remain valid. Consequently, except for extreme thermal wind, it is likely that the baroclinic model can be approximated by inclusion of thermal wind in the barotropic model. The validity of this postulate remains a matter to be tested.

It is not too difficult to visualize the limitation of the model due to the assumptions of steady-state barotropic and adiabatic conditions. Aside from these, the critical issue regarding the planetary boundary layer model is the assumption involved in expressing the stress in terms of the mean velocity. Here it was necessary to introduce the concepts of the mixing-length hypothesis. In some circles, the mixing-length hypothesis is in disfavor since it is based more on intuition than fundamentals. Nevertheless, the mixing-length approach has been successful in some areas of turbulence and it remains today the only practical approach for prediction models.

VI. COMPARISON WITH OTHER MODELS

Similar models based on the mixing-length hypothesis have been reported by Blackadar[4-5] and Lettau[9]. Each model is based on a slightly different mixing length and the equations were solved by different numerical methods. Lettau used a mixing length derived from duct flow and Blackadar used an empirical mixing length similar in form to the one used in this study.

A comparison of the drag coefficients and surface wind as functions of surface Rossby numbers from the three models is shown in Figures 10a and b. It can be seen that the three models give similar results. Comparing these results with the observation on Figure 5 indicates that one model cannot be singled out as being in better agreement with observations than the other.

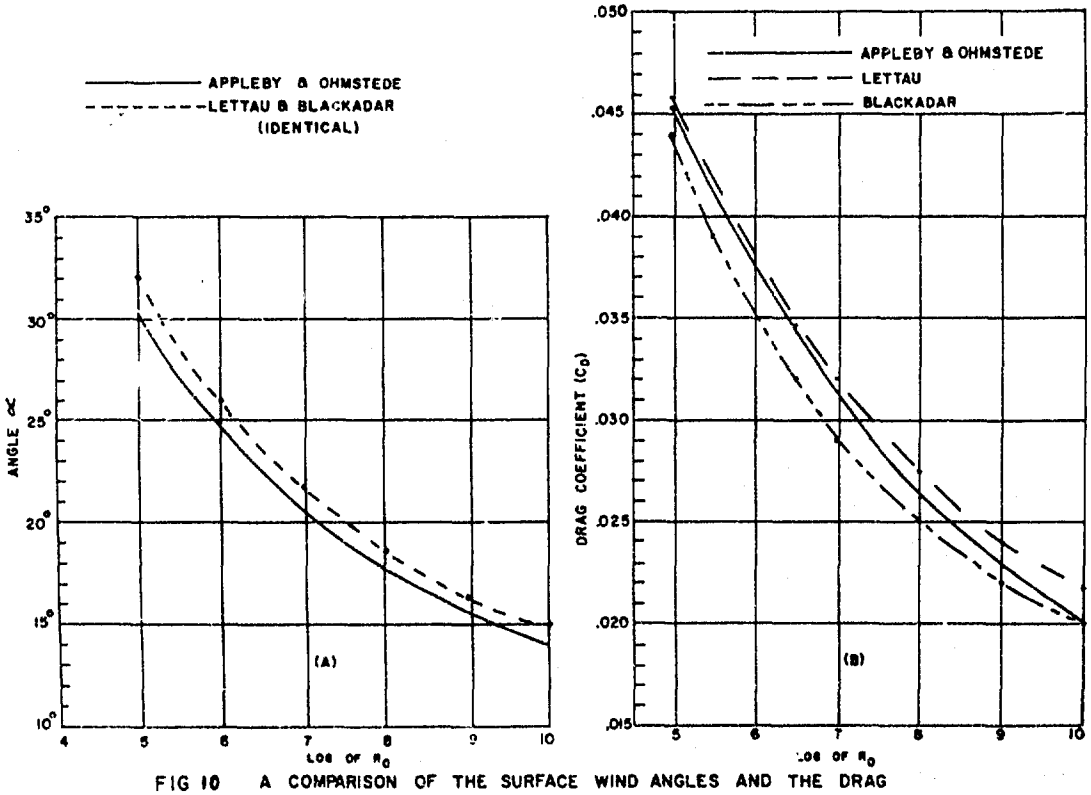

FIG 10 A COMPARISON OF THE SURFACE WIND ANGLES AND THE DRAG COEFFICIENTS PREDICTED BY THE THREE-MODELS.

VII. CONCLUSIONS

We believe that the development and solution of these planetary boundary layer models represents a significant step forward, since it furnishes a connecting link between micrometeorology and macrometeorology. We do not contend that the model presented is the final answer as it is based on several hypotheses which require experimental verification. The model is restricted to a class of atmospheric conditions. However, it represents a foundation which can be refined as more experimental data become available, and extended to cover a broader class of meteorological conditions.

The present model has strategic and design applications which require a knowledge of the distribution of wind or turbulence characteristics for differing situations. For example, it is believed that the model can be used to evaluate the effect of roughness on the diffusion of CBR agents. Such a study is now under way. In like manner, the model can be extended to a broader class of micrometeorological problems such as determining climatic and synoptic estimates of evapotranspiration from large-scale watersheds, and turbulent transfer of heat, water vapor, and carbon dioxide from the earth's surface.

From a long range standpoint, one of the great challenges facing meteorology is the development of a truly diabatic model for the prediction of the hemispheric circulation. An important feature of such a model would be the energy dissipation associated with the planetary boundary layer. The model furnishes estimates of the dissipation and surface shearing stress derived from knowledge of only the geostrophic wind, latitude and roughness.

It is concluded, therefore, that the planetary boundary layer model presented has useful applications and is worthy of extension to cover a broader class of situations.

APPENDIX A

Computation of Dimensional Parameters of the Boundary Layer

In order to compute dimensional parameters of the boundary layer, the geostrophic wind, latitude (Coriolis parameters) and surface roughness for the particular situation must be determined. Then the surface Rossby number and G/f can be computed. From Figure 4 the limiting mixing length (ℓ_o) and the boundary layer depth can be determined. The real height z can then be obtained from the z/ℓ_o column of Table II. The real wind components u and v for each level can be computed in two ways depending on the orientation desired. In the original orientation with the surface winds along the x axis, the following equations are applicable:

$$u = [\cos\alpha_o - r/r_o \cos\alpha\,]G \text{ and } v = [\sin\alpha_o - r/r_o \sin\alpha]G$$

If one desires to orient the geostrophic wind along the x axis, the equations are

$$u = [1 - r/r_o \cos(\alpha-\alpha_o)]G$$

$$v = [r/r_o \sin(\alpha-\alpha_o)]G$$

where r_o is the length of $\left[\left(\frac{G_x-u}{G}\right)^2_{z_o} + \left(\frac{G_y-v}{G}\right)^2_{z_o}\right]^{1/2}$ at the x_o/ℓ_o height and r is this quantity at specific levels; α_o is the angle between the surface and geostrophic wind; $\alpha = \arctan (G_y-v)/G/(G_y-v)/G$. To simplify the computation, values of r and α as functions of z/ℓ_o are given in Table IV. Figure 11 shows ℓ_o as a function of surface Rossby number; α_o can be found from Figure 10a.

The shearing stress components are obtained in a similar manner. First, the drag coefficient U*/G must be determined from Figure 10b; τ_o is then obtained from the equation $\tau_o = \rho\left(\frac{U*}{G}\right)^2 G^2$; τ_x and τ_y can be found from the following equations depending on the desired orientation. For the surface wind oriented along the x axis, the equations are

$$\tau_x = (t/t_o \cos\Psi)\tau_o$$

$$\tau_y = (t/t_o \sin\Psi)\tau_o$$

Table IV
r, t, α and Ψ as functions of z/ℓ_o

z/ℓ_o	r	α	$tx10^3$	Ψ
53.1	0	∞	0	∞
50.0	.0023	382.2	.0009	324.2
45.0	.0067	309.4	.0035	261.9
40.0	.0150	258.5	.0093	211.0
35.0	.0207	237.2	.0152	187.5
30.0	.0466	183.7	.0449	134.3
25.0	.0721	154.1	.0802	105.2
20.0	.1054	129.1	.1332	80.8
15.0	.1475	108.8	.2091	58.4
10.0	.2013	87.2	.3144	38.2
6.4	.2485	73.4	.4117	24.7
5.0	.2699	68.0	.4549	20.0
2.5	.3195	57.4	.5418	10.5
1.0	.3717	48.6	.5999	04.8
0.5	.4085	43.6	.6206	2.5
0.25	.4442	39.7	.6320	1.5
0.10	.4908	35.4	.6383	0.3
.01	.6440	26.6	.6413	0
.001	.7910	21.2	.6426	0
.0001	.9300	18.0	.6428	0
.00001	1.069	15.5	.6428	0
.000001	1.209	13.7	.6428	0

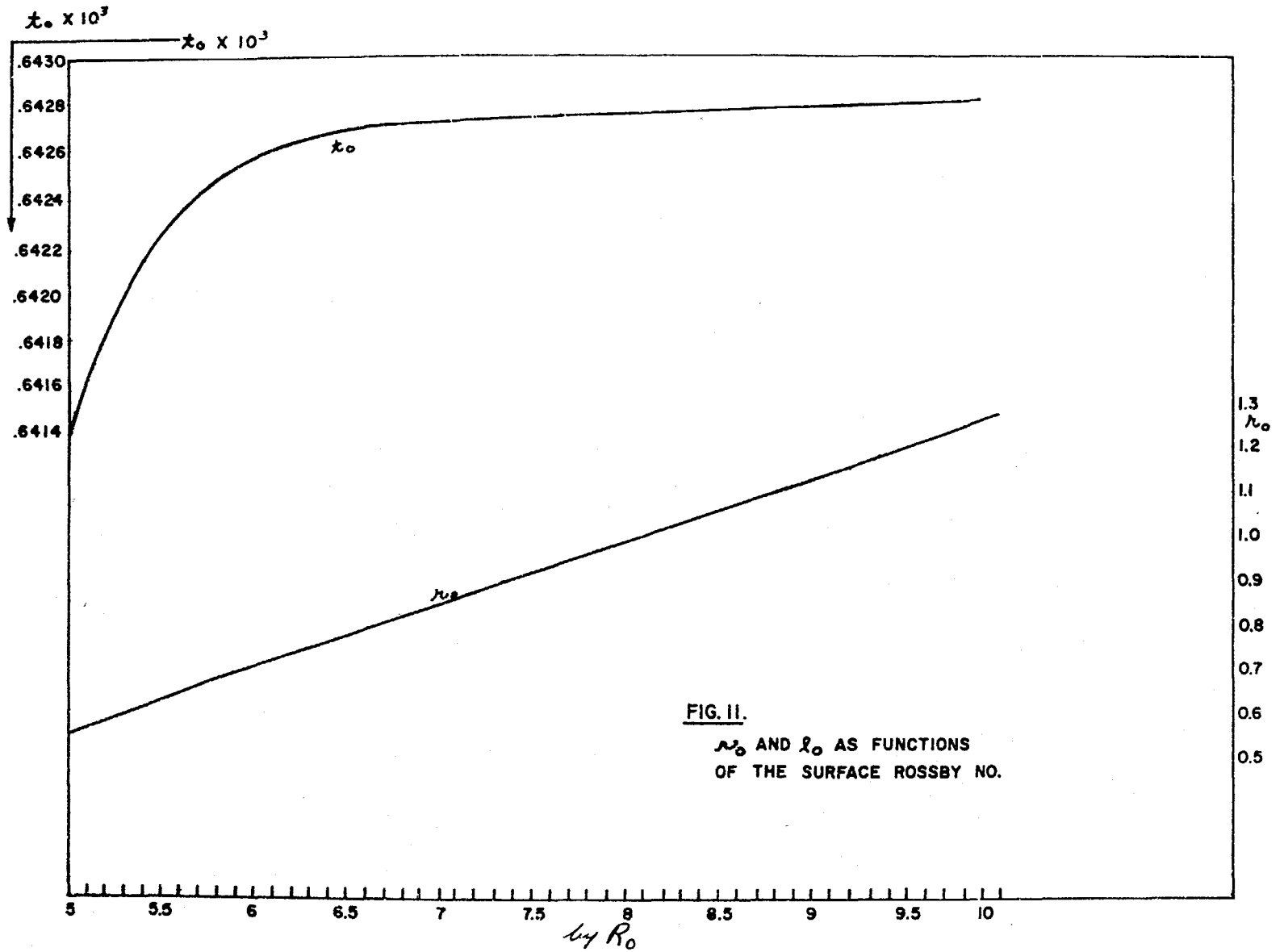

FIG. 11.

ν_o AND ℓ_o AS FUNCTIONS OF THE SURFACE ROSSBY NO.

For the geostrophic wind oriented along the x axis

$$\tau_x = t/t_o \cos(\alpha_o - \Psi)\tau_o$$

$$\tau_y = t/t_o \sin(\alpha_o - \Psi)\tau_o$$

where $t = [(\tau_x/\rho G^2)_z^2 + (\tau_y/\rho G^2)_z^2]^{1/2}$; t as a function of z/ℓ_o is given in Table IV and t_o is given in Figure 11 as a function of surface Rossby number; $\Psi = \arctan (\tau_y/\rho G^2)_z/(\tau_x/\rho G^2)_z$ is also given in Table IV as a function of z/ℓ_o ; $\Psi_o = 0$ and α_o is the angle of the surface wind with the geostrophic.

The friction velocity U_* is a scalar and can be found by multiplying the column U_*/G by a constant. The simplest method of determining the constant is to compute the ratio of the U_*/G given in Figure 10 for the desired surface Rossby number to the (U_*/G) in Table II for the required z_o/ℓ_o height. This ratio must be multiplied by G, the geostrophic wind speed.

Thus $$U_* = A \left(\frac{U_*}{G}\right)_{(z)}$$

where $$A = (U_*/G)_{R_o} / (U_*/G)_{z_o/\ell_o} \; G$$

To determine the distribution of K with height, the value of $K/\ell_o G$, found in the last column of Table II must also be multiplied by a constant. Since $K = U_* \ell$, the above constant (A) times ℓ_o is used.

Thus $$K = (K/\ell_o G)_z \; A\ell_o$$

A sample computation for all parameters of the Leipzig wind profile follows

geostrophic wind (G)	17.51 m/sec
surface roughness (z_o)	.20 m
Coriolis parameter (f)	$1.14 \times 10^{-4} \text{sec}^{-1}$
air density (ρ)	1.15×10^{-3}

$R_o = G/f \; z_o = 7.75 \times 10^5$; $\log R_o = 5.89$

$G/f = 1.538 \times 10^5$

To compute real height and depth of the boundary layer from Figure 4, $(Hf/G) \times 10^3 = 7.0$; $(\ell_o f/G) \times 10^4 = 2.1$

$$H = 1075;\ \ell_o = 32.3\ ;\ z_o/\ell_o = 6.19 \times 10^{-3}$$

To compute u, v, τ_x and τ_y

from Figure 10 $\alpha_o = 25.5$ and $U_*/G = .039 = C$

from Equation 25 $\tau_o = \rho C^2 G^2 = 5.36$ dynes/cm^2

from Figure 11 $r_o = .683$; $t_o = 0.64253 \times 10^{-3}$

To compute U_*

$$U_* = A\left(\frac{U_*}{G}\right)_z \quad \text{where } A = (U_*/G)_{R_o}/(U_*/G)_{z_o/\ell_o}\ G$$

from Table II, U_*G at z_o/ℓ_o of $6.19 \times 10^{-3} = .0253$

$$A = \frac{.039 \times 17.51}{.0253} = 27$$

$$U_* = 27 \times .0253 = .683 \text{ m/sec}$$

To compute K

$$K = (K/\ell_o G)_z\ A\ell_o$$

$$= .00009 \times 27 \times 32.3 = .078 \text{ m}^2/\text{sec}$$

Using these values, Table II and Table IV give the results shown in Table V. Figures 12 and 13 give a comparison of parameters derived from the model with those computed by Lettau [3,10] from the Leipzig profile.

Table V*
Leipzig Wind Profile Parameters* Computed from the Model

z(m)	U(m/sec)	V(m/sec)	τ_x(Dyn/cm^2)	τ_y(Dyn/cm^2)	U_*(m/sec)	K(m^2/sec)
1715.1	17.51	0	0	0	0	0
1615.0	17.51	-0.06	0	0	.024	.872
1453.5	17.47	-0.17	.02	.02	.051	1.659
1292.0	17.47	0.31	-.01	.00	.084	2.704
1130.5	17.96	-0.28	-.12	-.04	.105	4.099
969.0	18.62	0.44	-.12	-.35	.181	5.843
807.5	18.67	1.45	.12	-.66	.240	7.849
646.0	18.15	2.64	.63	-.91	.311	10.029
484.5	17.07	3.77	1.46	-.95	.389	12.558
323.0	15.05	4.56	2.55	-.62	.478	15.175
206.7	13.22	4.75	3.43	.05	.548	16.308
161.5	12.39	4.69	3.78	.36	.575	16.047
80.8	10.53	4.35	4.38	1.17	.629	12.820
32.3	8.71	3.75	4.68	1.77	.662	7.064
16.2	7.51	3.27	4.76	2.02	.672	3.924
8.1	6.47	3.00	4.81	2.14	.678	2.093
3.2	5.06	2.17	4.81	2.27	.680	.872
0.3	.93	0.32	4.83	2.30	.683	.078
0.2	0	0	4.84	2.31	.683	0

* Computed for a westerly geostrophic wind.

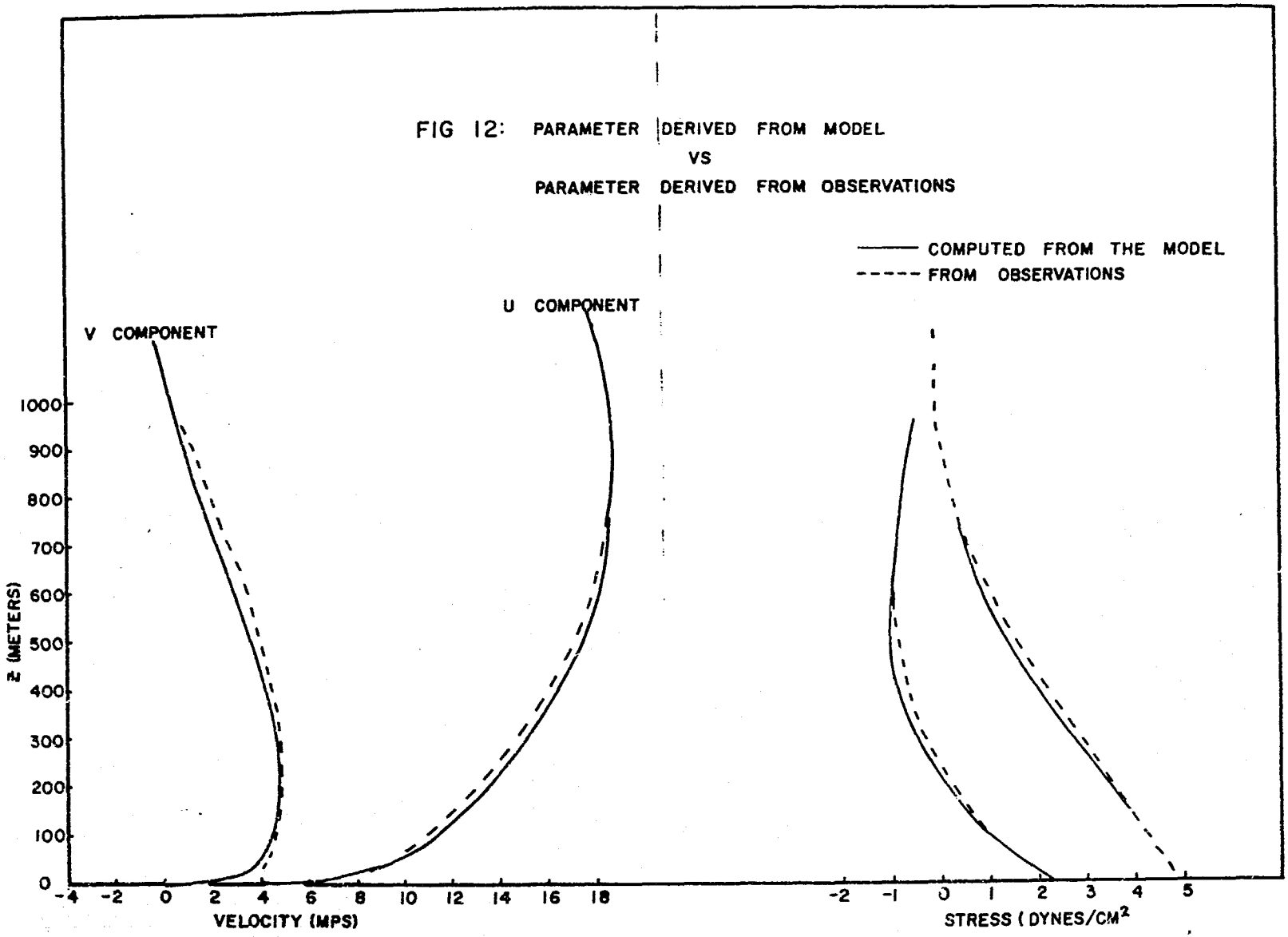
FIG 12: PARAMETER DERIVED FROM MODEL
VS
PARAMETER DERIVED FROM OBSERVATIONS
COMPUTED FROM THE MODEL
FROM OBSERVATIONS
V COMPONENT
U COMPONENT
Z (METERS)
1000
900
800
700
600
500
400
300
200
100
0
-4 -2 0 2 4 6 8 10 12 14 16 18
VELOCITY (MPS)
-2 -1 0 1 2 3 4 5
STRESS (DYNES/CM2

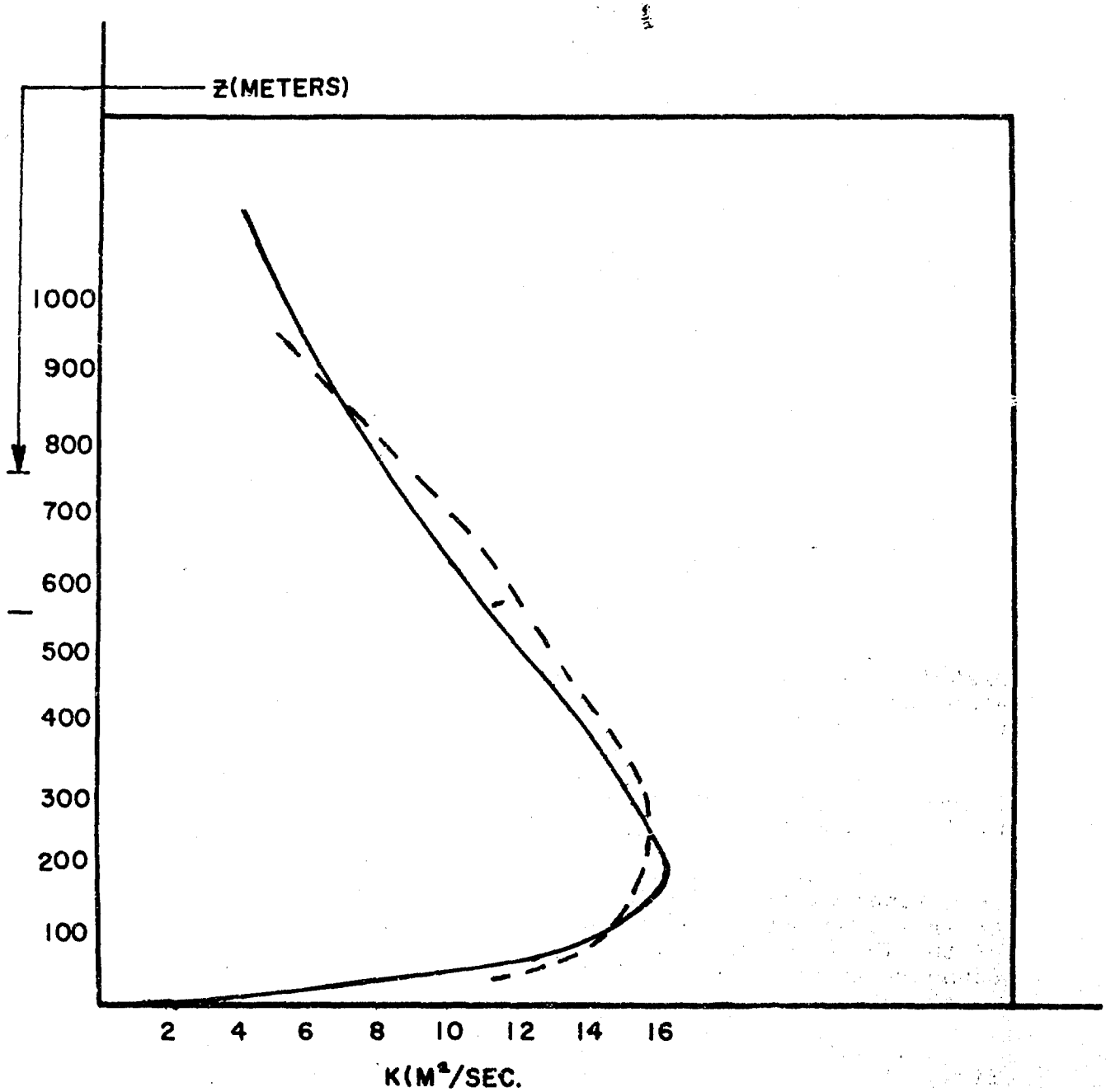

Fig 13 COMPARISON OF MODEL vs OBSERVED EDDY VISCOSITY (K) for LEIPZIG

BIBLIOGRAPHY

1. Lettau, H. H., "A Generalized Mathematical Model of the Mean-Velocity Distribution in Fully Turbulent Duct Flow," "Studies of the Three Dimensional Structure of the Planetary Boundary Layer," Annual Report, DA Contract 36-039-56-80282, August 1961.

2. Rossby, C. G. and Montgomery, R. B., "The Layer of Frictional Influence in Wind and Ocean Currents," Papers Phys. Oceanog. Meteorol., MIT and Woods Hole Oceanog, Inst., 3(3), 101 pp., 1935.

3. Lettau, H. H., "A Re-examination of the Leipzig Wind Profile Considering Some Relations Between Wind and Turbulence in the Friction Layer," Tellus, 2, 125-129, 1950.

4. Blackadar, Alfred K., "The Vertical Distribution of Wind and Turbulent Exchange in a Neutral Atmosphere," Journal of Geophysical Research, Vol 67, No. 8, 3095-3102, 1962.

5. Blackadar, Alfred K., "The Vertical Distribution of Wind in a Baroclinic Adiabatic Atmospheric Boundary Layer," 211th National Meeting of the American Meteorolo. Soc. 21-24 Jan 63.

6. U. S. Weather Bureau, "Meteorology and Atomic Energy," prepared for the U. S. Atomic Energy Commission, U. S. Government Printing Office, July 1955.

7. Kung, E. G., and Lettau, H. H., "Regional and Meridional Distribution of Continental Vegetational Cover and Aerodynamic Roughness Parameters," "Studies of the Three Dimensional Structure of the Planetary Boundary Layer," Annual Report, DA Contract 36-039-56-80282, August 1961.

8. Lettau, H. H., "Wind Profile, Surface Stress, Etc., Atmospheric Diffusion and Air Pollution," Symp. Proc., Oxford, 24-29 August 1958, 241-257, Advances in Geophysics, Vol 6, Academic Press 1959.

9. Lettau, H. H., "Theoretical Wind Spirals in the Boundary Layer of a Barotropic Atmosphere," "Studies of the Three Dimensional Structure of the Planetary Boundary Layer," Annual Report, DA Contract 36-039-56-80282, August 1961.

CONT'd BIBLIOGRAPHY

10. _____"Notes on the Transformation of Mechanical Energy from and to Eddying Motion." J. of Meteorol., 11, 196-201, 1954.

DISTRIBUTION LIST USAERDAA-MET-5-64

	No Cys
1. Commanding General U. S. Army Materiel Comd ATTN: AMCRD-RS-ES-A Washington, D. C. 20315	1
2. Commanding General U.S. Army Materiel Comd ATTN: AMCRD-DE-MI Washington, D. C., 20315	1
3. Chief, Rsch & Development Department of the Army ATTN: CRD/M Washington, D. C. 20315	2
4. Commanding General USA Combat Development Comd ATTN: CDCMR-E Fort Belvoir, Va. 22060	1
5. Commanding General U.S. Continental Army Comd ATTN: ATINT-P&O Fort Monroe, Virginia 23351	1
6. Chief, Comm-Electronics Department of the Army Washington, D. C. 20315	1
7. Commanding General U.S. Army Electronics Comd ATTN: AMSEL-RE-C Fort Monmouth, N. J. 07703	2
8. Commanding General U.S. Army Missile Command Physical Sciences Laboratory ATTN: Dr. Oskar M. Essenwanger AMSMI-RRA, Bldg. 5429 Redstone Arsenal, Ala. 35809	2
9. Commanding General U.S. Army Munitions Comd ATTN: AMSMU-RC Dover, New Jersey 07801	2
10. Commanding General U.S. Army Mobility Comd ATTN: Research Div Centerline, Mich. 48015	2
11. Commanding General U.S. Army T&E Comd ATTN: Directorate NBC Testing Aberdeen Proving Ground, Md 21005	2
12. Commanding Officer USA Cold Region R&D Lab ATTN: Environmental Rsch Br Hanover, N. H. 03755	2
13. Commanding General U.S. Army GSR&E Laboratory ATTN: Earth Sciences Div Natick, Mass. 01760	2
14. Commanding Officer U.S. Army Ballistic Rsch Labs ATTN: AMXBR-B Aberdeen Proving Ground, Md 21005	2
15. Director USA Eng Waterways Expr Sta ATTN: WESSR Vicksburg, Miss. 39181	1
16. Commanding Officer U.S. Army Elec R&D Agency ATTN: Met Div, Survl Dept Fort Monmouth, N.J. 07703	2
17. Commanding Officer U.S. Army Elec R&D Activity ATTN: Missile Meteorology Div White Sands Msl Range, N.M. 88002	2
18. Commanding Officer U.S. Army Biological Labs ATTN: CB Cloud Rsch Office Fort Detrick, Frederick, Md.	1
19. Commanding Officer U.S. Army Frankford Arsenal ATTN: MEIE Div Philadelphia, Pa. 19103	1
20. Commanding Officer Picatinny Arsenal ATTN: Special Weapons Group Dover, New Jersey 07801	1
21. Commanding Officer U. S. Army Engnr R&D Lab Fort Belvoir, Virginia 22060	1
22. Commanding Officer USA Transportation Rsch Comd Fort Eustis, Virginia 23604	1
23. Commanding Officer U.S. Army Dugway Proving Grnd ATTN: Meteorology Div Dugway, Utah 84002	1
24. President U.S. Army Artillery Bd Fort Sill, Okla. 73504	1
25. Commanding Officer U.S. Army Arty Development Agcy Fort Sill, Okla. 73504	1
26. Commanding Officer U.S. Army Comm-Elct CDC Agcy Fort Huachuca, Arizona 85613	1
27. Commandant U.S. Army Arty & Msl School ATTN: Target Acquisition Dept Fort Sill, Okla. 73504	1
28. Commander Air Weather Service (MATS) ATTN: AWSSS/TIPD Scott AFB, Ill. 62226	1
29. Commander AF Cambridge Rsch Labs ATTN: CRXL, Hanscom Field Bedford, Mass. 01730	2

DISTRIBUTION LIST USAERDAA-MET-5-64

		No Cys
30.	Chief of Naval Research ATTN: CODE 427 Department of Navy Washington, D. C. 20315	1
31.	U.S. Naval Weather Service U.S. Naval Air Station Washington, D. C. 20315	1
32.	Officer-in-Charge U.S. Naval Weather Rsch Fac U.S. Naval Air Sta. Bldg R28 Norfolk, Virginia 23501	1
33.	Director Atmospheric Science Programs National Science Foundation Washington, D. C. 20315	1
34.	Director Bureau of Rsch & Development Federal Aviation Agency Washington, D. C. 20315	1
35.	Natl Avn Facilities Exper Cen Federal Aviation Agency ATTN: Tech Library, Bldg 3 Atlantic City, N. J. 08401	1
36.	Chief, Fallout Studies Br Div of Biology and Medicine Atomic Energy Commission Washington, D. C. 20315	1
37.	Asst Sec of Defense R&D The Pentagon ATTN: Tech Library, Rm 3E1065 Washington, D. C. 20315	1
38.	Director, Met Systems Office of Applications (FM) Natl Aeronautics & Space Adm Washington, D.C. 20315	1
39.	Chief, U.S. Weather Bureau ATTN: Librarian (24th/M Sts) Washington, D. C. 20315	2
40.	Commanding Officer Defense Documentation Center Cameron Sta, Alexandria, Va 22314	20
41.	Robt A. Taft Sanitary Engn Cen Public Health Service 4676 Columbia Parkway Cincinnati, Ohio 45202	1
42.	Chief, Bu Naval Weapons Department of the Navy CODE: FASS Washington, D.C. 20315	1
43.	Commanding Officer U.S. Army Elec R&D Activity ATTN: Meteorology Dept Fort Huachuca, Ariz. 85613	50
44.	Commander USAF Cambridge Rsch Labs ATTN: CRZW 1065 Main Street Waltham, Mass. 02154	1
45.	Commanding General Deseret Test Center Fort Douglas, Utah 84113	1
46.	Commanding Officer U.S. Army Arctic Test Cen Fort Greely, Alaska	1
47.	Commanding General U.S. Army T&E Comd ATTN: AMSTE-EL Aberdeen P.G. Md 21005	1
48.	Commanding General U.S. Army T&E Comd ATTN: AMSTE-BAF Aberdeen P.G., Md 21005	1
49.	Commanding General U.S. Army Missile Comd ATTN: AMSMI-RB Redstone Arsenal, Ala. 35809	1
50.	Commanding Officer U.S. Army Biological Labs ATTN: SMUFD-12-TI Ft. Detrick, Fredrick,Md 21701	1
51.	Commanding General U.S. Army Missile Comd ATTN: AMSMI-RR Redstone Arsenal, Ala. 35809	1
52.	Commanding Officer USA CBR Operations Rsch Gp Army Chemical Cen, Md. 21210	1
53.	Commanding Officer US Army Chemical R&D Labs ATTN: Director, Development Spt Army Chemical Center, Md. 21210	1
54.	Chief, Comm-Electronics Department of the Army ATTN: Technical Director, Comd & Con Sys Directorate Washington, D. C. 20315	1
55.	Scientific & Tech Info Agcy ATTN: NASA Rep (S-AK/DL) P.O. Box 5700 Bethesda, Md. 20014	1
56.	Commanding Officer U.S. Army Polar R&D Center Fort Belvoir, Va 22060	1
57.	Commanding General CDC Experimentation Cen Fort Ord, Calif. 93941	1
58.	Director, Meteorology Dept University of Arizona Tucson, Ariz 85717	1

DISTRIBUTION LIST USAERDAA-MET-5-64

		No Cys
59.	Director U.S. Water Conservation Lab Agricultural Rsch Svc, USDA Route 2, Box 816-A Tempe, Arizona 85281	1
60.	Director Pac SW Forest & Range Ex Sta USDA Forest Service, Box 245 Berkeley, Calif. 94704	1
61.	Director, Meteorology Dept Univ of California at L.A. Los Angeles, Calif 90052	1
62.	Director, U.S. Salinity Lab P. O. Box 672 ATTN: Dr. Richards Riverside, Calif. 92502	1
63.	Department of Irrigation University of California Davis, Calif. 95616	1
64.	Dept of Agricultural Engng University of California ATTN: Dr. F.A. Brooks Davis, Calif. 95616	1
65.	Meteorology Department San Jose State College San Jose, Calif. 95113	1
66.	Chief, Radio Propagation Lab U.S. Natl Bureau of Standards Boulder, Colo. 80301	1
67.	Librarian Natl Cen for Atmospheric Rsch Boulder, Colo. 80301	1
68.	Dept of Civil Engineering Colorado State University Fort Collins, Colo. 80521	1
69.	Forest Service Exper Sta Colorado State University ATTN: M. Martinelli, Jr. Rm 221, Forestry Bldg Fort Collins, Colo. 80521	1
70.	Director, Meteorology Dlpt Florida State University Tallahassee, Florida 32301	1
71.	Director, USDA Field Sta (Southern Piedmont Soil Consvtn) P. O. Box 33 Watkinsville, Georgia 30677	1
72.	Meteorology Department University of Hawaii Honolulu, Hawaii 96822	1
73.	Director, Meteorology Dept University of Chicago Chicago, Illinois 60607	1
74.	Department of Agronomy Iowa State University ATTN: Dr. R.H. Shaw Ames, Iowa 50010	1
75.	Director Soil & Water Consvtn Div Agricultural Rsch Svc (USDA) Beltsville, Md. 20705	1
76.	Director Department of Civil Engng John Hopkins University Baltimore, Md. 21233	1
77.	Executive Secretary American Met Society 45 Beacon Street Boston, Mass. 02109	1
78.	Round Hill Field Station Mass. Institute of Technology South Dartmouth, Mass. 02748	1
79.	Director, Meteorology Dept Mass. Institute of Technology Cambridge, Mass. 02138	1
80.	Director, Meteorology Dept University of Michigan Ann Arbor, Mich. 48105	1
81.	University of Minnesota ATTN: Dean Spilhaus Minneapolis, Minn. 55041	1
82.	Natl Severe Storm Project Federal Office Bldg (Rm 710) 911 Walnut Street ATTN: Library Kansas City, Mo. 64108	1
83.	Director, Meteorology Dept St. Louis University St. Louis, Mo. 63120	1
84.	Department of Soils University of Missouri Columbia, Mo. 62501	1
85.	Department of Geophysics Washington University St. Louis, Mo. 63120	1
86.	Director, Meteorology Dept New York University University Heights New York, N. Y. 10001	1
87.	Soil & Water Consvtn Rsch Div Agricultural Rsch Svc (USDA) Cornell Univ, Bailey Hall Ithaca, N. Y. 14851	1
88	Scientific Rsch Institute Oregon State College ATTN: ATmospheric Sciences Br Corvallis, Oregon 97330	1

DISTRIBUTION LIST USAERDAA-MET-5-64

		No Cys
59.	Director U.S. Water Conservation Lab Agricultural Rsch Svc, USDA Route 2, Box 816-A Tempe, Arizona 85281	1
60.	Director Pac SW Forest & Range Ex Sta USDA Forest Service, Box 245 Berkeley, Calif. 94704	1
61.	Director, Meteorology Dept Univ of California at L.A. Los Angeles, Calif 90052	1
62.	Director, U.S. Salinity Lab P. O. Box 672 ATTN: Dr. Richards Riverside, Calif. 92502	1
63.	Department of Irrigation University of California Davis, Calif. 95616	1
64.	Dept of Agricultural Engng University of California ATTN: Dr. F.A. Brooks Davis, Calif. 95616	1
65.	Meteorology Department San Jose State College San Jose, Calif. 95113	1
66.	Chief, Radio Propagation Lab U.S. Natl Bureau of Standards Boulder, Colo. 80301	1
67.	Librarian Natl Cen for Atmospheric Rsch Boulder, Colo. 80301	1
68.	Dept of Civil Engineering Colorado State University Fort Collins, Colo. 80521	1
69.	Forest Service Exper Sta Colorado State University ATTN: M. Martinelli, Jr. Rm 221, Forestry Bldg Fort Collins, Colo. 80521	1
70.	Director, Meteorology Dlpt Florida State University Tallahassee, Florida 32301	1
71.	Director, USDA Field Sta (Southern Piedmont Soil Consvtn) P. O. Box 33 Watkinsville, Georgia 30677	1
72.	Meteorology Department University of Hawaii Honolulu, Hawaii 96822	1
73.	Director, Meteorology Dept University of Chicago Chicago, Illinois 60607	1
74.	Department of Agronomy Iowa State University ATTN: Dr. R.H. Shaw Ames, Iowa 50010	1
75.	Director Soil & Water Consvtn Div Agricultural Rsch Svc (USDA) Beltsville, Md. 20705	1
76.	Director Department of Civil Engng John Hopkins University Baltimore, Md. 21233	1
77.	Executive Secretary American Met Society 45 Beacon Street Boston, Mass. 02109	1
78.	Round Hill Field Station Mass. Institute of Technology South Dartmouth, Mass. 02748	1
79.	Director, Meteorology Dept Mass. Institute of Technology Cambridge, Mass. 02138	1
80.	Director, Meteorology Dept University of Michigan Ann Arbor, Mich. 48105	1
81.	University of Minnesota ATTN: Dean Spilhaus Minneapolis, Minn. 55041	1
82.	Natl Severe Storm Project Federal Office Bldg (Rm 710) 911 Walnut Street ATTN: Library Kansas City, Mo. 64108	1
83.	Director, Meteorology Dept St. Louis University St. Louis, Mo. 63120	1
84.	Department of Soils University of Missouri Columbia, Mo. 62501	1
85.	Department of Geophysics Washington University St. Louis, Mo. 63120	1
86.	Director, Meteorology Dept New York University University Heights New York, N. Y. 10001	1
87.	Soil & Water Consvtn Rsch Div Agricultural Rsch Svc (USDA) Cornell Univ, Bailey Hall Ithaca, N. Y. 14851	1
88	Scientific Rsch Institute Oregon State College ATTN: ATmospheric Sciences Br Corvallis, Oregon 97330	1

DISTRIBUTION LIST USAERDAA-MET-5-64

		No Cys
89.	Director, Meteorology Dept Pennsylvania State Univ University Station, Pa. 16802	1
90.	Dept of Oceanography & Met Texas A&M College College Station, Texas 77840	1
91.	Electrical Engng Rsch Lab University of Texas Austin, Texas 78761	1
92.	Department of Agronomy Utah State University ATTN: Dr. S.A. Taylor Logan, Utah 84321	1
93.	Dept of Meteorology University of Utah Salt Lake City, Utah 84116	1
94.	Director, Natl Rsch Council Natl Academy of Sciences 2101 Constitution Ave Washington, D. C. 20315	1
95.	Director, Meteorology Dept University of Washington Seattle, Wash. 99703	1
96.	Director, Meteorology Dept University of Wisconsin Madison, Wisconsin 53705	1
97.	Department of Soils University of Wisconsin ATTN: Dr. C.B. Tanner Madison, Wisc. 53705	1
98.	Commander U.S. Navy Electronics Lab ATTN: Dr. M. Halstead San Diego, Calif 92101	1
99.	Officer-in-Charge Meteorological Curriculum U.S. Naval Post Graduate Sch Monterey, Calif. 92801	1
100.	Director, Geophysical Rsch USAF Cambridge Rsch Cen ATTN: CRZHB (Hanscom Field) Bedford, Mass. 01730	2
101.	Commandant U.S. Army Sig Cen & Sch ATTN: Weather Branch DST Fort Monmouth, N. J. 07703	1
102.	Commanding Officer U.S. Army Electronics Labs Fort Monmouth, N. J. 07703	1
103.	Deputy for Defense R&E Office of SECDEF ATTN: Geophysical Sciences Washington, D. C. 20315	1
104.	USAF Climatic Center Air Weather Svc (MATS) ATTN: CCCAD Annex 2, 225 D. St., S.E. Washington, D. C. 20315	1
105.	Forestry Library 260 Walter Mulford Hall University of California Berkeley, Calif. 94704	1
106.	Commanding General U.S. Army Edgewood Arsenal ATTN: Operations Rsch Gp Edgewood Arsenal, Md. 21040	1
107.	Commanding Officer U.S. Army Tropic Test Center P.O. Drawer 942 ATTN: Chief Scientist Fort Clayton, C. Z.	1
108.	Commander AF Cambridge Rsch Labs ATTN: Chief, Boundary Layer Br Bedford, Mass. 01730	1
109.	Argonne National Lab ATTN: Mr. Harry Moses Meteorology Bldg. 9700 South Cass Avenue Argonne, Ill. 60440	1
110.	Commanding Officer U.S. Army Chemical School ATTN: Micromet Br. Tech Div Ft. McClellan, Ala. 36205	1
111.	Director Transport Dept 315 Bloor Street, West Toronto 5, Ontario,Canada	1
112.	Dept of Soil Science Ontario Agricultural College Guelph Ontario, Canada	1
113.	Iowa State University of Science & Technology ATTN: Agronomy Dept Ames, Iowa 50010	1
114.	Brookhaven National Lab ATTN: Meteorology Group Upton Long Island, N. Y.	1
115.	Commanding Officer U.S. Army Tropic Test Center ATTN: STERO-RE Fort Clayton, C. Z.	1
116.	Director National Security Agency ATTN: [illegible] Ft. George G. Meade, Md. 20755	1

UNCLASSIFIED

Security Classification

DOCUMENT CONTROL DATA - R&D

(Security classification of title, body of abstract and indexing annotation must be entered when the overall report is classified)

1 ORIGINATING ACTIVITY *(Corporate author)*

U.S. Army Electronics Research & Development Activity, (USAERDAA) Ft. Huachuca, Arizona 85613

2a. REPORT SECURITY CLASSIFICATION

Unclassified

2b. GROUP

N/A

3. REPORT TITLE

NUMERICAL SOLUTION OF THE DISTRIBUTION OF WIND AND TURBULENCE IN THE PLANETARY BOUNDARY LAYER (U)

4 DESCRIPTIVE NOTES *(Type of report and inclusive dates)*

5. AUTHOR(S) *(Last name, first name, initial)*

Appleby, James F., and Ohmstede, William D.

6. REPORT DATE	7a. TOTAL NO. OF PAGES	7b. NO. OF REFS
September 1964	47	10

8a. CONTRACT OR GRANT NO.	9a. ORIGINATOR'S REPORT NUMBER(S)
b. PROJECT NO. 1V0-14501-B-53A	USAERDAA-MET-5-64
c. Task No. 1V0-14501-B-53A-08	9b. OTHER REPORT NO(S) *(Any other numbers that may be assigned this report)*
d.	Meteorological Rsch Notes No. 8

10. AVAILABILITY/LIMITATION NOTICES

Qualified requesters may obtain copies of this report from DDC.

11. SUPPLEMENTARY NOTES	12. SPONSORING MILITARY ACTIVITY
	Meteorology Department, USAERDAA Ft. Huachuca, Arizona

13. ABSTRACT

The objective of this study is to develop a theoretical model for the structure of turbulence in the atmosphere and to solve the equations for the distribution of wind and turbulence in the planetary boundary layer. Starting with the basic equation of motion for an incompressible fluid, it is modified to incorporate the mixing-length hypothesis of Prandtl to relate the turbulent stresses to the mean flow characteristics. It is assumed the atmosphere is adiabatic, barotropic, and in a steady state. These assumptions are not all essential to the solution but do simplify the discussion. Based on the assumptions, a relation for the mixing-length distribution within the boundary layer is developed. Using this relationship in the equation of motion led to a set of second order, nonlinear differential equations, which were solved on a digital computer. Universal profiles of the wind, stress, and eddy viscosity were fixed by invoking the important notion of similarity, that is, it is assumed the scale of turbulence is uniquely related to the gross dimensions of the boundary layer. The requisite universal constant is evaluated from experimental data. Possible applications of the model to practical problems are outlined.

DD FORM 1 JAN 64 1473

UNCLASSIFIED

Security Classification

14. KEY WORDS	LINK A		LINK B		LINK C	
	ROLE	WT	ROLE	WT	ROLE	WT
Micrometeorology Numerical Solutions Planetary Boundary Layer Wind and Turbulence Distribution Dissipation Eddy Viscosity Mixing Length						

INSTRUCTIONS

1. ORIGINATING ACTIVITY: Enter the name and address of the contractor, subcontractor, grantee, Department of Defense activity or other organization *(corporate author)* issuing the report.

2a. REPORT SECURITY CLASSIFICATION: Enter the overall security classification of the report. Indicate whether "Restricted Data" is included. Marking is to be in accordance with appropriate security regulations.

2b. GROUP: Automatic downgrading is specified in DoD Directive 5200.10 and Armed Forces Industrial Manual. Enter the group number. Also, when applicable, show that optional markings have been used for Group 3 and Group 4 as authorized.

3. REPORT TITLE: Enter the complete report title in all capital letters. Titles in all cases should be unclassified. If a meaningful title cannot be selected without classification, show title classification in all capitals in parenthesis immediately following the title.

4. DESCRIPTIVE NOTES: If appropriate, enter the type of report, e.g., interim, progress, summary, annual, or final. Give the inclusive dates when a specific reporting period is covered.

5. AUTHOR(S): Enter the name(s) of author(s) as shown on or in the report. Enter last name, first name, middle initial. If military, show rank and branch of service. The name of the principal author is an absolute minimum requirement.

6. REPORT DATE: Enter the date of the report as day, month, year; or month, year. If more than one date appears on the report, use date of publication.

7a. TOTAL NUMBER OF PAGES: The total page count should follow normal pagination procedures, i.e., enter the number of pages containing information.

7b. NUMBER OF REFERENCES: Enter the total number of references cited in the report.

8a. CONTRACT OR GRANT NUMBER: If appropriate, enter the applicable number of the contract or grant under which the report was written.

8b, 8c, & 8d. PROJECT NUMBER: Enter the appropriate military department identification, such as project number, subproject number, system numbers, task number, etc.

9a. ORIGINATOR'S REPORT NUMBER(S): Enter the official report number by which the document will be identified and controlled by the originating activity. This number must be unique to this report.

9b. OTHER REPORT NUMBER(S): If the report has been assigned any other report numbers *(either by the originator or by the sponsor)*, also enter this number(s).

10. AVAILABILITY/LIMITATION NOTICES: Enter any limitations on further dissemination of the report, other than those imposed by security classification, using standard statements such as:

(1) "Qualified requesters may obtain copies of this report from DDC."

(2) "Foreign announcement and dissemination of this report by DDC is not authorized."

(3) "U. S. Government agencies may obtain copies of this report directly from DDC. Other qualified DDC users shall request through _____."

(4) "U. S. military agencies may obtain copies of this report directly from DDC. Other qualified users shall request through _____."

(5) "All distribution of this report is controlled. Qualified DDC users shall request through _____."

If the report has been furnished to the Office of Technical Services, Department of Commerce, for sale to the public, indicate this fact and enter the price, if known.

11. SUPPLEMENTARY NOTES: Use for additional explanatory notes.

12. SPONSORING MILITARY ACTIVITY: Enter the name of the departmental project office or laboratory sponsoring *(paying for)* the research and development. Include address.

13. ABSTRACT: Enter an abstract giving a brief and factual summary of the document indicative of the report, even though it may also appear elsewhere in the body of the technical report. If additional space is required, a continuation sheet shall be attached.

It is highly desirable that the abstract of classified reports be unclassified. Each paragraph of the abstract shall end with an indication of the military security classification of the information in the paragraph, represented as *(TS), (S), (C), or (U).*

There is no limitation on the length of the abstract. However, the suggested length is from 150 to 225 words.

14. KEY WORDS: Key words are technically meaningful terms or short phrases that characterize a report and may be used as index entries for cataloging the report. Key words must be selected so that no security classification is required. Identifiers, such as equipment model designation, trade name, military project code name, geographic location, may be used as key words but will be followed by an indication of technical context. The assignment of links, rules, and weights is optional.